FENOC
FirstEnergy Nuclear Operating Company

Davis-Besse Nuclear Power Station
5501 North State Route 2
Oak Harbor, Ohio 43449-9760

Howard W. Bergendahl
Vice President - Nuclear

419-321-8588
Fax: 419-321-8337

Docket Number 50-346

License Number NPF-3

Serial Number 1-1280

July 12, 2002

Mr. James E. Dyer, Administrator
United States Nuclear Regulatory Commission
Region III
801 Warrenville Road
Lisle, IL 60532-4351

Subject: Confirmatory Action Letter: Response to Request for Additional Information Related to the Davis-Besse Nuclear Power Station Safety Significance Assessment

Dear Mr. Dyer:

This letter responds to the June 24, 2002 (Log Number 5980) NRC staff request for additional information (RAI) related to the Safety Significance Assessment of the Davis-Besse Nuclear Power Station (DBNPS) Reactor Pressure Vessel Head as was submitted by FirstEnergy Nuclear Operating Company letter Serial Number 1-1268 dated April 8, 2002. The RAI included questions from the Office of Nuclear Reactor Regulation and the Office of Nuclear Regulatory Research.

Should you have any questions or require additional information, please contact Mr. Patrick J. McCloskey, Manager - Regulatory Affairs, at (419) 321-8450.

Very truly yours,

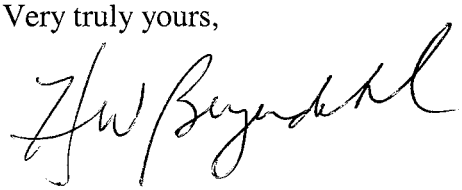

MKL

Enclosures

cc: USNRC Document Control Desk
D. V. Pickett, NRC/NRR Project Manager
S. P. Sands, NRC/NRR Backup Project Manager
C. S. Thomas, NRC Region III, DB-1 Senior Resident Inspector
Utility Radiological Safety Board

RESPONSE TO REQUEST FOR ADDITIONAL INFORMATION

REGARDING THE APRIL 8, 2002

SAFETY SIGNIFICANCE ASSESSMENT

FOR

DAVIS-BESSE NUCLEAR POWER STATION
UNIT NUMBER 1

FAILURE CRITERION

Question 1:

What is the technical basis of the failure criterion (e.g., strain exceeding 11.15 percent) used to determine the failure conditions of the cladding layer? Provide specific technical references in the literature that support the failure criterion used in this evaluation.

DBNPS Response to Question 1:

The strain value of 11.15% corresponds to the uniform elongation of the stress-strain curve used in the evaluation. The use of this value as the basis for the failure criterion is based largely on engineering judgment. The premise is that when any section in the cladding has through-wall strains greater than the uniform elongation, then that section has no more capacity of resisting any additional increase in load. This criterion is judged to be conservative because in reality, there is redistribution of stresses and strains to adjacent elements that would prevent incipient failure when the strains in a particular column of elements exceed this criterion.

Furthermore, it should be noted that the value of uniform elongation used in the evaluation (11.15%) is very conservative for stainless steel weld metal. Data obtained from the literature, and summarized in Table 1 indicates that the average uniform elongation for submerged arc welds (SAW) is 25.7% and that for shielded metal arc welds (SMAW) is 30.7%. The average for both populations is 27.3%. Most of the data shown in Table 1 indicate uniform elongation greater than 20% with only two data points below this value.

Subsequent to the publication of Structural Integrity report W-DB-01Q-301 (Reference 1), an evaluation of the reasonableness of the failure criterion was performed, W-DB-01Q-304 (Reference 2), using disk burst test data (Reference 3). A copy of the evaluation is attached. The disk burst test data is included as Appendix B to the evaluation. The conclusion of the evaluation is that the failure criterion is conservative compared to the disk burst test results. The burst test pressures were also compared to the pressures at which numerical instability occurred

during the elastic-plastic analysis and it was found that the instability pressures, although slightly under-predicting the test failure pressures, are a much better predictor of failure pressure than any of the proposed strain-based failure criteria.

Base on the above information and data, it is believed that the use of the 11.15% uniform elongation as a basis for the failure criterion is very conservative.

Table 1: Tensile Test Data for 304 Stainless Steel at 550 °F

Reference	Yield Strength (ksi)	Ultimate Tensile Strength (ksi)	Uniform Elongation (%)	Reduction in Area (%)	Material Type
NUREG/CR-6235	20.8	62	38.4	70.8	Base
NUREG/CR-4538	22.2	67.3	39	70.8	Base
NUREG/CR-4538	22.8	68.8	40.5	70.8	Base
NUREG/CR-4687	20.1	65.2	53.8	71.3	Base
EPRI NP-4768	23.1	61.3	47	74	Base
EPRI NP-4768	24.8	62.6	45	70	Base
EPRI NP-4768	33.2	72.7	42	67	Base
ASME 72PVP12	34	84	54	75	Base
		Ave.Base	**45.0**	**71.2**	
EPRI NP-4668	44.8	62.9	22	46	SAW
EPRI NP-4768	36	61.8	25	67	SAW
EPRI NP-4768	40.8	70.3	25	69	SAW
NUREG/CR-6098	37.4	68	26.4		SAW
NUREG/CR-6389	49.1	68.1	30	46	SAW
NUREG/CR-6389	45	67.1	33	42.4	SAW
NUREG/CR-6389	54.3	74	15.5	63	SAW
NUREG/CR-6389	51.8	71.8	13.7	54	SAW
NUREG/CR-4878	47.1	67.6	31.5	44.2	SAW
NUREG/CR-4878	28.3	67.5	34.5	47	SAW-Annealed
		Ave.SAW	**25.7**	**53.2**	
EPRI NP-4668	45.7	65.1	26	58	SMAW
EPRI NP-4768	46.8	61.4	37	48	SMAW
EPRI NP-4768	49.4	64.7	35	46	SMAW
NUREG/CR-4878	40.8	70.3	24.8	68.6	SMAW
		Ave.SMAW	**30.7**	**55.2**	
NUREG/CR-4538	44.3	65.4	33	74.3	Weld
NUREG/CR-4538	42.2	64.3	30	72.9	Weld
		Ave.SAW&SMAW	**27.3**	**53.8**	

Question 2:

How does the failure criterion (e.g., based on ultimate strain in a uniaxial tensile test) account for the effects of biaxial loading in the cladding, or triaxial loading in the cladding at the edges of the degradation cavity?

DBNPS Response to Question 2:

The failure criterion was based solely on the uniform elongation and did not consider biaxial or triaxial effects. Nevertheless, as discussed in the response to Question 1, the criterion is conservative compared to burst test results on test specimens that are similar to the exposed cladding in the degradation cavity geometry.

Question 3:

The failure criterion applied in Structural Integrity Analysis (SIA) report W-DB-01Q-301 (e.g., the minimum cross-sectional strain exceeding the failure strain of 11.15 percent) allows the strain levels in the cladding to exceed the critical strain value entirely through the thickness, leading to very large strains at the surface of the cladding, up to 49 percent in Table 5 of the SIA report. What is the technical basis for this approach, as opposed to the average cross-sectional strain, or the maximum cross-sectional strain?

DBNPS Response to Question 3:

Even though the failure criterion used resulted in some elements in the cross-section exceeding the failure strain, the criterion, as compared to actual burst test data, was found to be conservative (see response to Question 1).

Question 4:

Did you explore a continuum damage mechanics analysis to give guidance of the failure criterion once the strains exceed the critical strain where necking/void growth starts? If not, provide the technical basis for not using a continuum damage mechanics analysis. [Poisson's ratio of 0.5 no longer applies once this critical strain level is exceeded, so the analysis is strictly not valid. (Poisson's ratio is continuously changing as the voids grow at the strains beyond the start of necking.) This results in a stress redistribution that is not accounted for in a standard elastic-plastic analysis.]

DBNPS Response to Question 4:

The analysis performed was judged to be conservative as validated by the disk burst test results discussed in the response to Question 1, and as such, it was judged unnecessary to consider the application of continuum damage mechanics analysis to this evaluation.

Question 5:

How would the strain values change if the stress free temperature was assumed to be the stress relief temperature instead of 70 °F, and the analysis accounted for the differential thermal expansion of the cladding and head steel at the operating temperature of 605 °F?

DBNPS Response to Question 5:

As can be seen in the Structural Integrity report W-DB-01Q-301, and as further clarified by the above responses to Questions 1 through 4, the strains at the failure pressures from both the analyses and experiments are very large (on the order of 11% or greater). The strains corresponding to thermal expansion effects, at either temperature, are expected to be much smaller (on the order of 0.1%). Therefore, the effects of changing from a stress free temperature of 70 °F to 605 °F will not have any significant impact on the results of the analysis.

GEOMETRY/MESHING

Question A:

Does the size of the degradation cavity and the transition from the cladding thickness to the head thickness that was used in the SIA report reflect current knowledge regarding the cavity geometry, in particular the undercut area described in Figure 13 on page 103 of the Davis-Besse Root Cause Analysis Report (CR 2002-0891), dated April 15, 2002? What is the transition geometry assumed in the analyses?

DBNPS Response to Question A:

The size of the degradation cavity and the transition from the cladding thickness to the head thickness used in the calculation reflected what was the best available at the time of the calculation. More work is currently in progress on the removed damaged cavity to determine the exact size and geometry of the cavity and transition regions.

Question B:

Is there sufficient mesh refinement through the cladding thickness to adequately capture the bending and shear strains at the edge of the cavity? Describe any sensitivity studies used to demonstrate the adequacy of the mesh refinement.

Response to Question B:

In the analysis of the cavity, six elements were used through the thickness of the cladding. A convergence study, using both an axisymmetric model and a three dimensional model was performed in Reference 2 to evaluate the impact of the number of through-wall elements in the thickness of the test specimens. The results indicate that there is no significant difference in the burst pressure predictions when the number of through-wall elements is increased from six to 12. Therefore, it is concluded that the analyses of the categories with six elements though the thickness represents a converged solution. Furthermore, when fewer elements than six were used in the convergence study, it resulted in conservative estimates of the burst pressures.

Question C:

Was the cladding deposited by weld wire? Do the thinner cladding thickness measurements from ultrasonic testing coincide with the locations of weld bead toes? In what direction do the cladding weld beads run relative to the long axis of the degradation?

DBNPS Response to Question C:

The cladding was deposited by weld wire. It is difficult to determine if the thinner cladding thickness measurements from the UT coincided with the location of the weld bead toes since the UT measurements were taken on one-inch grids and as such, there was not adequate resolution to make such a determination. It is also difficult to determine the direction of the cladding weld beads from the available information. Additional investigation of the removed cavity is currently in progress that might provide more information.

References

1) Structural Integrity Calculation W-DB-01Q-301, Rev. 1, "Elastic-Plastic Finite Element Stress Analysis of Davis-Besse RPV Head Wastage Cavity."

2) Structural Integrity Calculation W-DB-01Q-304, Rev. 0, "Evaluation of Failure Criterion Used in Elastic-Plastic Analysis of Davis-Besse RPV Wastage."

3) P. C. Riccardella, "Elastic-Plastic Analysis of Constrained Disk Burst Tests," ASME Paper No. 72-PVP-12, Proceedings of Pressure Vessel and Piping Conference, New Orleans, LA, September 17-21, 1972.

Docket Number 50-346
License Number NPF-3
Serial Number 1-1280
Enclosure 1
Attachment

Structural Integrity Calculation W-DB-01Q-304

(39 pages attached)

STRUCTURAL INTEGRITY Associates, Inc.	CALCULATION PACKAGE	FILE No: W-DB-01Q-304 PROJECT No: W-DB-01Q

PROJECT NAME: Operability and Root Cause Evaluation of the Damage of the Reactor Pressure Vessel Head at Davis-Besse

CLIENT: First Energy Corporation

CALCULATION TITLE: Evaluation of Failure Criterion Used in Elastic-Plastic Analysis of Davis-Besse RPV Head Wastage

PROBLEM STATEMENT OR OBJECTIVE OF THE CALCULATION:

Develop a finite element model to simulate actual test data to evaluate the effectiveness of the failure criteria used in the elastic-plastic stress analysis of Davis-Besse RPV head wastage cavity.

Document Revision	Affected Pages	Revision Description	Project Mgr. Approval Signature & Date	Preparer(s) & Checker(s) Signatures & Date
0	1 – 28 A1 – A2 B1 – B9 Project CD-Rom	Original Issue	6/25/02	RLB 6-25-02 6/28/02

1.0 Introduction

During recent in-service inspections of the reactor pressure vessel (RPV) head and penetrations at Davis-Besse, significant wastage was observed in the vicinity of control rod drive mechanism (CRDM) No. 3. A calculation package was prepared for First Energy [1] to determine the limiting pressure load of the damaged RPV head.

Based on the review of this calculation package, the NRC raised a number of questions (See Appendix A), the majority of which were concerned with the failure criteria used in the evaluations.

The purpose of this calculation is to develop a better understanding of the failure criteria as used and its relative "conservativeness" in regards to the failure pressure.

2.0 Technical Approach

The failure criterion used in Reference 1 was set such that the maximum strain could not exceed the ultimate tensile strain. Hence for the stainless steel cladding where the maximum strain is expected to occur, the maximum equivalent total strain is limited to the maximum strain of 11.15% (corresponding to the ultimate strain for the stainless steel cladding in Reference 2) through the thickness of the component.

In order to evaluate the reasonableness of this failure criterion, the results of the failure pressures predicted with this criterion were compared against test results of very similar geometries. Disk burst test, similar to the Davis-Besse head wastage geometry were performed under the auspices of the PVRC Subcommittee and documented in and ASME publication [3] (see Appendix B for the actual publication).

Described in Reference 3 were a series of burst tests using machined disks of various materials. The test disk dimensions and the illustration of the test setup are shown in Figure 1. The materials tested included 304 Stainless Steel, A-533 Grade B Low Alloy Steel and ABS-C Carbon Steel. For the purposes of this calculation, only the 304 Stainless Steel testing will be reviewed.

As can be seen in Figure 1, three basic disk geometries were tested. In order to evaluate the effectiveness of the failure criteria developed for Reference 1, the same failure criteria will be used to determine the disk burst pressures. As a result, a series of finite element models were developed using the test disk dimension provided in Reference 3. The models were created and evaluated using the ANSYS finite element software [4]. The actual evaluations and subsequent failure criteria comparison are included in the following sections.

3.0 Finite Element Models

A series of finite element models were constructed to determine burst pressure for the various disk configurations. Initial studies were performed using an axisymmetric model but subsequent evaluations included three-dimensional modeling similar to that used in Reference 1.

The elastic material properties for all evaluations were for 304 stainless at room temperature as defined by Reference 5. These values used were as follows:

Modulus of Elasticity, E, e^6 psi:	28.3
Poisson's Ration, ν:	0.3

The plastic material properties for stainless per Reference 3 were:

0.25 Y.S. (psi)	**S_{ult} (psi)**	**ε_{ult} (in/in)**	**Reduction In Area**	**$A^{[1]}$ (psi)**	**$n^{[1]}$**
34,000	84,000	0.54	0.74	193,060	0.494

[1] Stress Strain Curve Assumed to be of form $\sigma = A (\varepsilon)^n$

Therefore the stress-strain curve used in all of the evaluation is shown in Table 1. Any additional model specific conditions will be described in the following sections.

Table 1
Stress Strain Curve for 304 Stainless Steel [3]

Strain (in.in)	Stress (psi)
0.000	0
0.025	31208.63
0.050	43952.49
0.075	53699.79
0.100	61900.24
0.125	69113.97
0.150	75627.79
0.175	81611.83
0.200	87176.84
0.225	92399.68
0.250	97336.26
0.275	102028.8
0.300	106510
0.325	110805.8
0.350	114937.5
0.375	118922.4
0.400	122775
0.425	126507.5
0.450	130130.6
0.475	133653.1
0.500	137083
0.525	140427.1
0.550	143691.6
0.575	146881.9
0.600	150002.7
0.625	153058.4
0.650	156052.8
0.675	158989.5
0.700	161871.6
0.725	164702.2
0.750	167483.7
0.775	170218.7
0.800	172909.5
0.825	175558
0.850	178166.2
0.875	180735.8
0.900	183268.6
0.925	185766
0.950	188229.5
0.975	190660.4
1.000	193060
1.025	195429.4
1.050	197769.7
1.075	200082
1.100	202367.3
1.125	204626.4
1.150	206860.2
1.175	209069.7
1.200	211255.4
1.225	213418.2

3.1 Axisymmetric Finite Element Model

The axisymmetric models were developed in ANSYS using the 2-D 8-Node Structural Solid element, PLANE82. All three geometries described in Reference 3 were evaluated as was the effects of the finite element mesh density on the onset of numeric instability. A total of 5 evaluations for each disk geometry were made, the only difference between each evaluation was the mesh density, which can be simplified to the number of elements through the thickness of the thinned portion of the disk. As such, the mesh densities that were evaluated where 4, 6, 8, 10 and 12 elements through the thickness. Figure 2 shows the progression of mesh density for geometry-A.

The mechanical boundary conditions for these evaluations consisted of simple vertical restraint throughout the approximate clamp region. This region was assumed to be the portion of the disk that remained at the full 1 inch thickness. See Figure 3 for an example of the applied boundary conditions on the 4 element through thickness, geometry-A model.

3.2 Three-Dimensional Finite Element Model

The three-dimensional models were developed in ANSYS using the 3-D 8-Node Structural Solid element, SOLID45. All three geometries described in Reference 3 were evaluated as was the effects of the finite element mesh density on the onset of numeric instability.

Only a 30° section of the total disk was modeled since the loading and geometries were also symmetrical. Two evaluations for each disk geometry were made; the only difference between each evaluation was the mesh density, which again can be simplified to the number of elements through the thickness of the thinned portion of the disk. As such, the mesh densities for the 3-dimensional models that were evaluated were 4 and 6 elements through the thickness. It should be noted that the stainless clad for the actual Davis-Besse cavity evaluation [1] used 6 elements through the thickness. Figure 4 shows the two mesh densities for geometry-A.

The mechanical boundary conditions for these evaluations used the same vertical restraints as the axisymmetric evaluations. In addition, symmetric boundary conditions were applied to the outside radial section surface of the disk, the preventing translations in the circumferential direction. This results in the centerline of nodes being limited to translation in only the vertical direction See Figure 5 for an example of the applied boundary conditions on the 4 element through thickness, geometry-A model.

4.0 Loading

All of the evaluations were loaded in the same manner. An incremental pressure was applied to the cavity surfaces until instability was reached. See Figure 6 for an example of the applied pressure.

5.0 Mesh Density Results

For each evaluation, the pressure was allowed to rise incrementally until instability occurred. The points of instability, as compared to the actual disk burst tests, are shown in Table 2.

Table 2
Mesh Density Effects of Numeric Instability

Model		Pressure (psi)		Predicted/ Test Result (%)
Model Type	Through-Wall Elements	Numeric Instability	Actual Test Burst	
Geometry-A Models				
Axisymmetric	4	12725	15000	84.8
Axisymmetric	6	13942		92.9
Axisymmetric	8	14004		93.4
Axisymmetric	10	14022		93.5
Axisymmetric	12	14005		93.4
3-Dimensional	4	13979		93.2
3-Dimensional	6	13997		93.3
Geometry-B Models				
Axisymmetric	4	5929	6800	87.2
Axisymmetric	6	6638		97.6
Axisymmetric	8	6695		98.5
Axisymmetric	10	6695		98.5
Axisymmetric	12	6694		98.4
3-Dimensional	4	6688		98.4
3-Dimensional	6	6671		98.1
Geometry-C Models				
Axisymmetric	4	6317	7700	82.0
Axisymmetric	6	6962		90.4
Axisymmetric	8	6997		90.9
Axisymmetric	10	6998		90.9
Axisymmetric	12	6997		90.9
3-Dimensional	4	6976		90.6
3-Dimensional	6	6974		90.6

The results are also shown graphically in Figure 7.

6.0 Total Strain Results

Based on Section 5, only the highest through-wall element count cases will be further evaluated. As a result, Figures 8 though 10 show the total Von Mises Strain just prior to onset of instability for the 12 through-wall element axisymmetric model and Figures 11 through 13 show total Von Mises Strain for the 6 through-wall element 3-D model.

7.0 Strain Criteria Comparison

The original failure strain criterion described in Section 2.0 indicated that when the through-wall total strain exceeded the uniform elongation percentage, the structure would be considered to have failed. As a check of this criterion, the total Von Mises nodal strains as they varied with pressure were extracted from the middle of the modeled disk at the top, middle and bottom of the wall thickness. The resulting strains were then plotted versus the pressure and compared to the actual burst pressure measured in Reference 3 and the failure pressure as defined by the Failure Criterion in Section 2.0.

From the definition of material properties used in the disk burst test, the uniform elongation for 304 stainless steel was 54% (see Section 3.0). Therefore, the failure of the disk will occur when the through-wall total strain exceeds 54% throughout the thickness.

An examination of the 3 geometries for both the axisymmetric and 3-D modeling can be seen in Figures 14 though 19. The results are further summarized in Table 3.

Table 3
Failure Criteria Comparison

Model Type	Model Geometry	Failure Pressure (psi)		
		Burst Test [3]	Instability	Failure Criteria
Axisymmetric	A	15000	14005	~11000
Axisymmetric	B	6800	6694	~5500
Axisymmetric	C	7700	6997	~5750
3-Dimensional	A	15000	13997	~11000
3-Dimensional	B	6800	6671	~5500
3-Dimensional	C	7700	6974	~5750

8.0 Conclusions

Based on the summary in Table 3 of Section 7.0, the use of the uniform elongation limit as the basis of failure criteria in an elastic-plastic finite element analysis results in conservative failure pressures as compared to actual test results. For the three geometries, the uniform elongation criteria predicted a failure pressure that was in the range of 73% to 81% of the actual failure pressure.

A better prediction of actual failure pressure is the pressure at which instability was reached in the ANSYS program. Assuming a instability criterion, failure pressure would range from 90% to 98% of actual failure pressure.

9.0 References

1) Structural Integrity Calculation W-DB-01Q-301, Rev. 1, "Elastic-Plastic Finite Element Stress Analysis of Davis-Besse RPV Head Wastage Cavity."

2) Email of from B.R. Grambau (Framatome ANP) to N. Cofie (SI), "308 Stress –Strain Curve," March 15, 2002, SI File W-DB-01Q-202.

3) P. C. Riccardella, "Elastic-Plastic Analysis of Constrained Disk Burst Tests," ASME Paper No. 72-PVP-12, Proceedings of Pressure Vessel and Piping Conference, New Orleans, LA, September 17-21, 1972.

4) ANSYS/Mechanical, Revision 5.7, ANSYS Inc., December 2000

5) ASME Boiler and Pressure Vessel Code, Section II, Part D, 1998 Edition

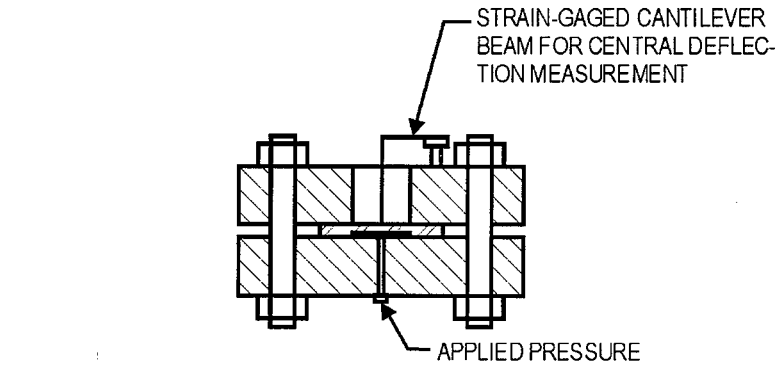

SCHEMATIC ILLUSTRATION OF TEST SETUP

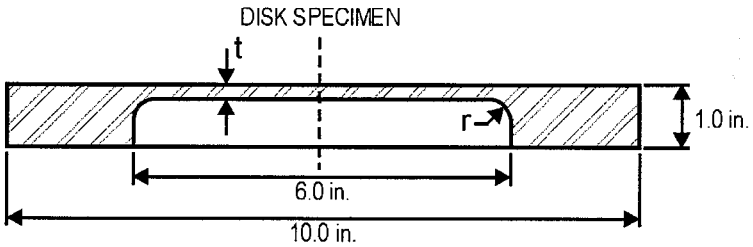

GEOMETRY	THICKNESS (t)	FILLET RADIUS ®
A	0.25 in.	0.375 in.
B	0.125 in.	0.125 in.
C	0.125 in.	0.375 in.

02055R0

Figure 1 – PVRC Disk Test Details (Reference 3)

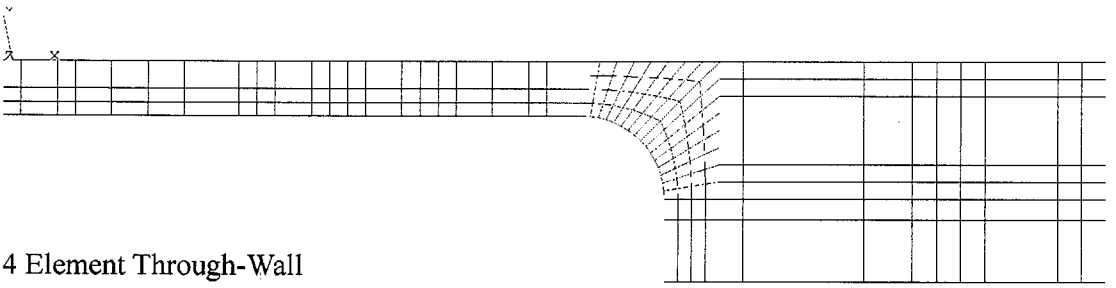

4 Element Through-Wall

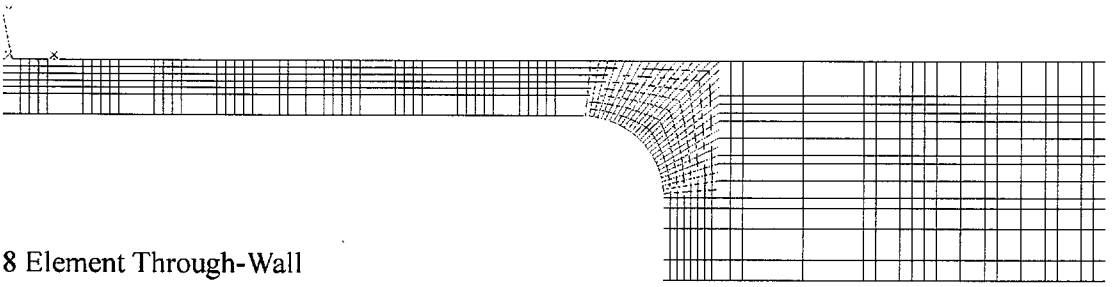

8 Element Through-Wall

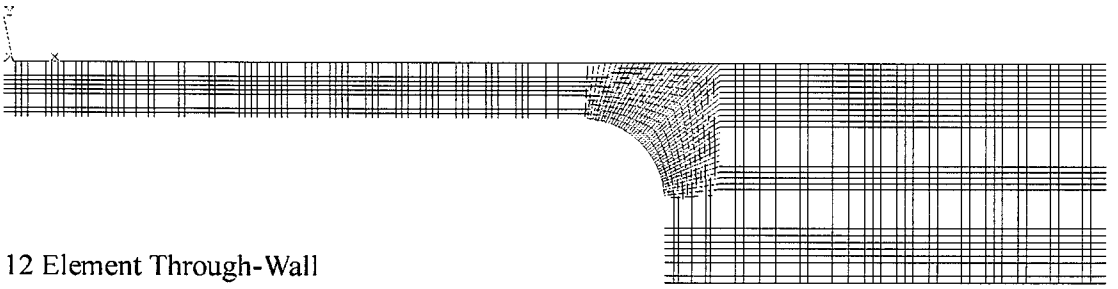

12 Element Through-Wall

Figure 2 – Mesh Density Example for Axisymmetric Finite Element Model for Geometry-A

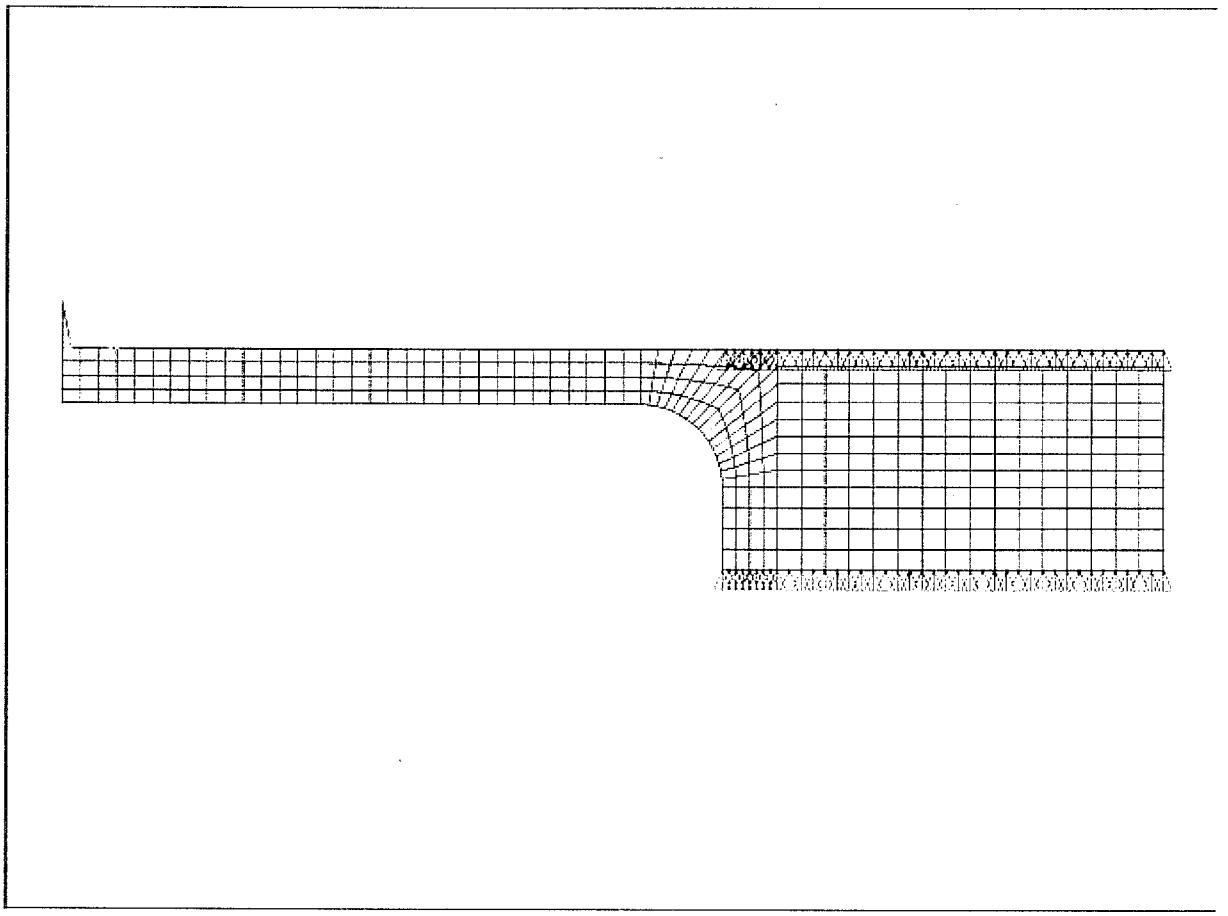

Figure 3 – Mechanical Boundary Conditions Example for Axisymmetric Finite Element Model for Geometry-A

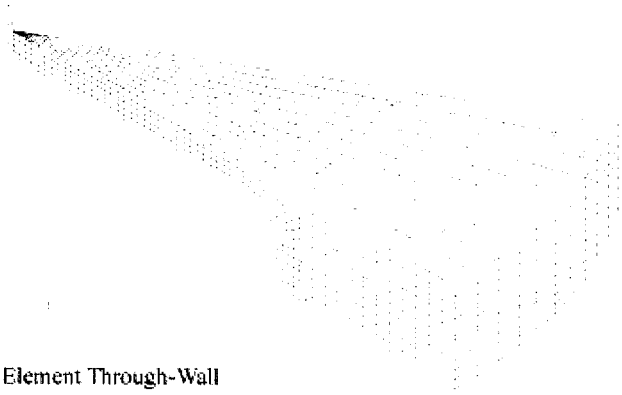

4 Element Through-Wall

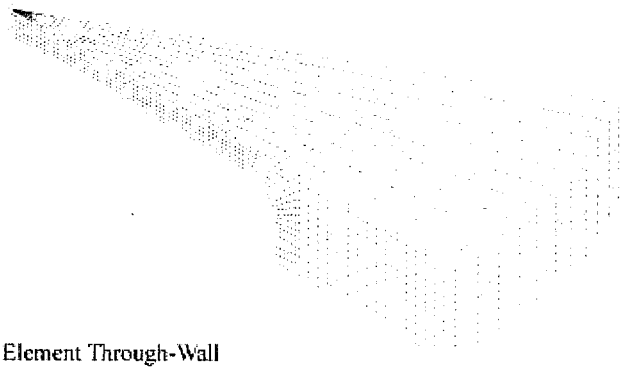

6 Element Through-Wall

Figure 4 – Mesh Density Example for 3-D Finite Element Model for Geometry-A

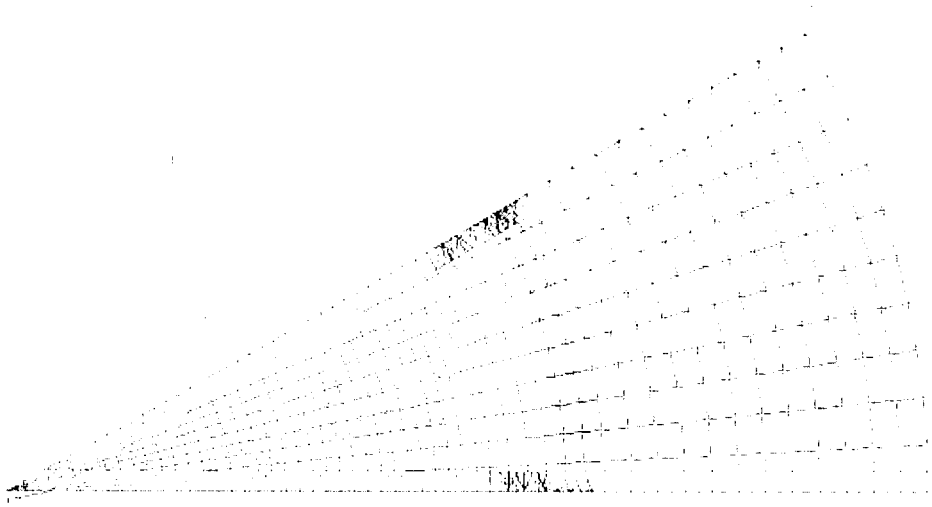

Figure 5 – Mechanical Boundary Conditions Example for 3-D Finite Element Model for Geometry-A

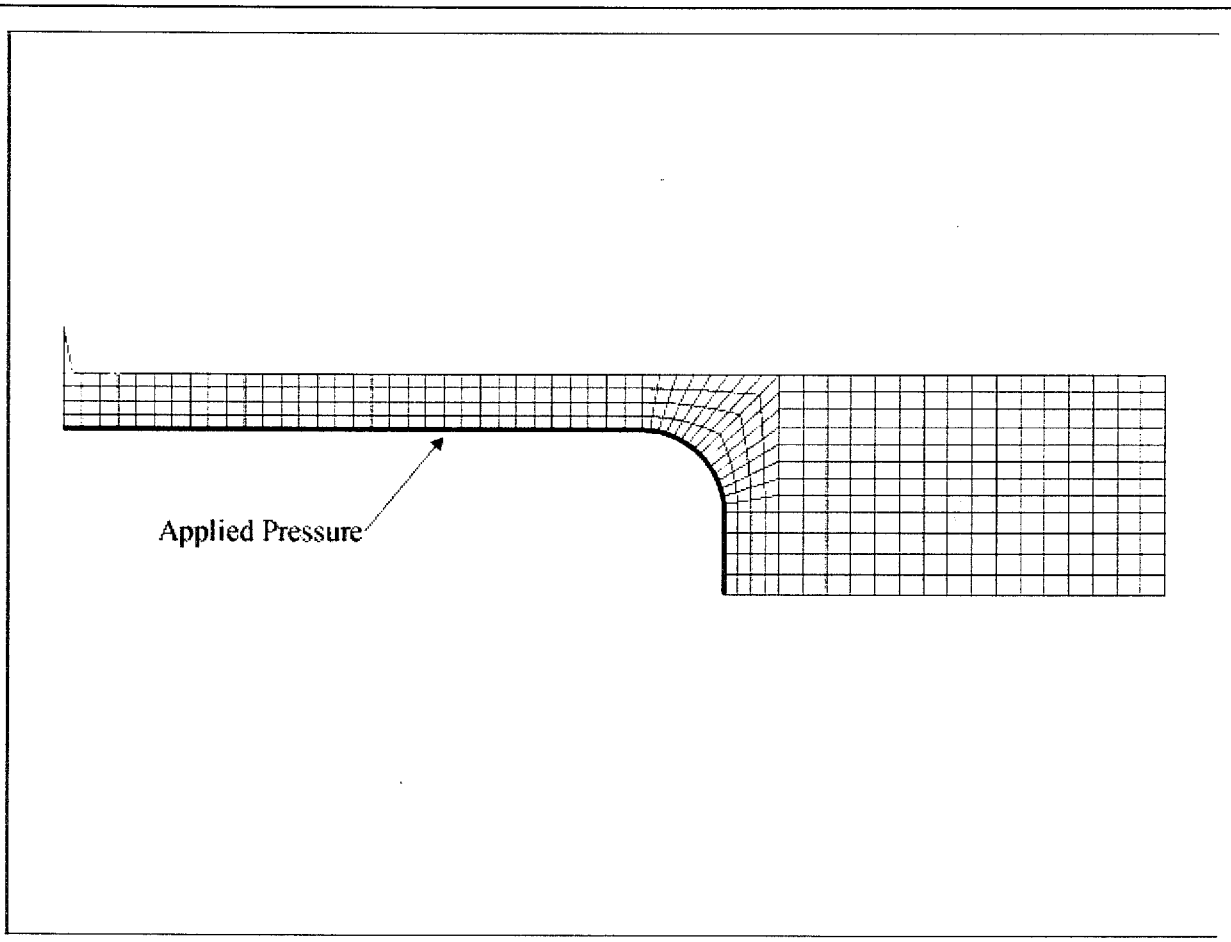

Figure 6 – Applied Pressure Example (Axisymmetric Geometry-A Model)

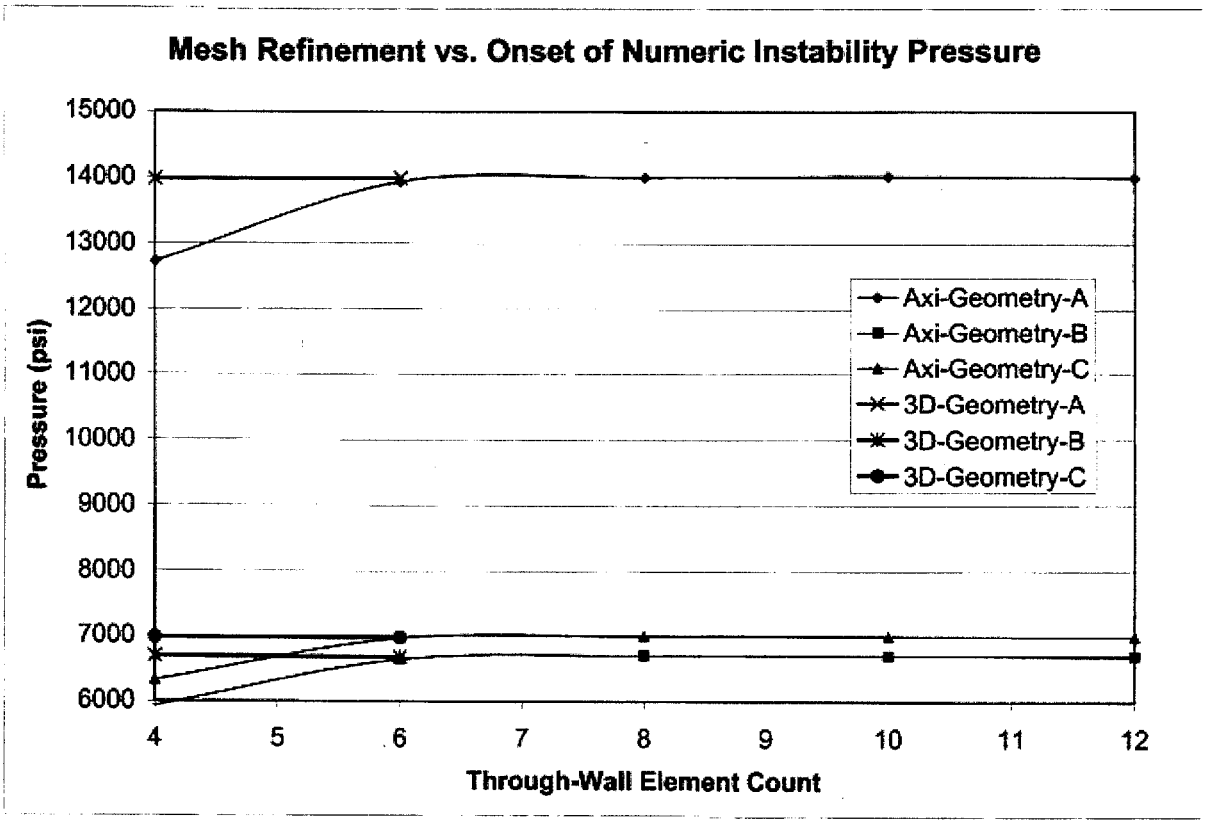

Figure 7 – Mesh Density Effects

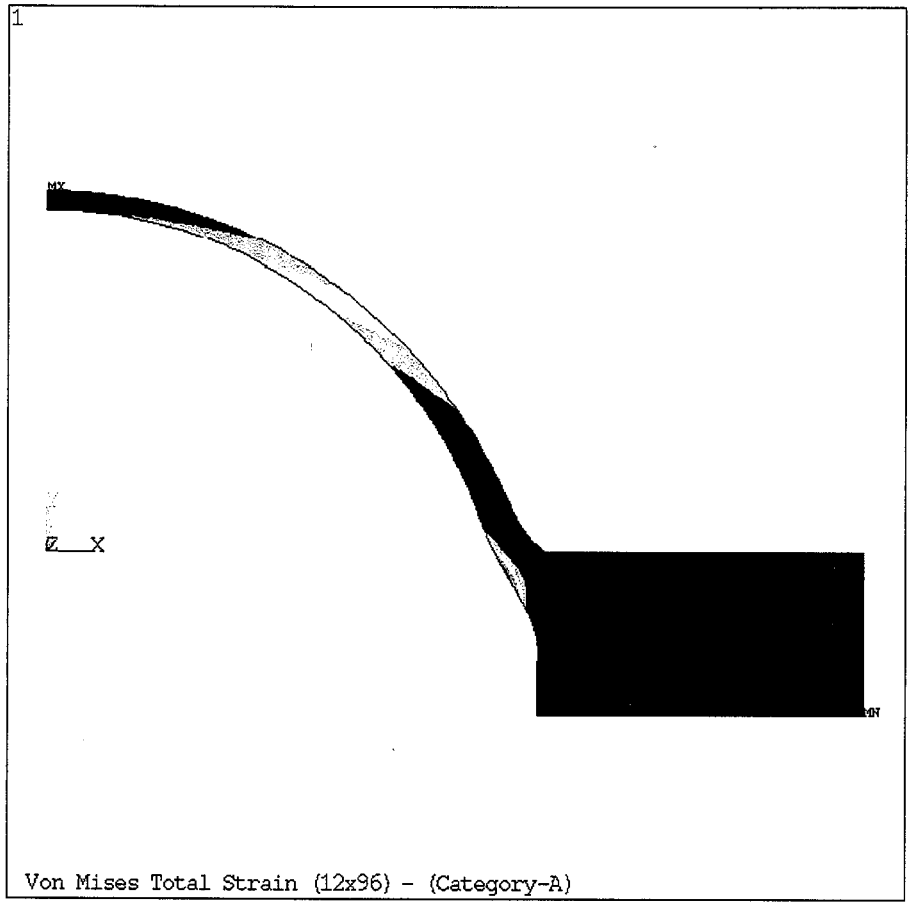

Figure 8 – Total Von Mises Strain Just Prior to Numeric Instability
Geometry-A – Axisymmetric (12 Elements)

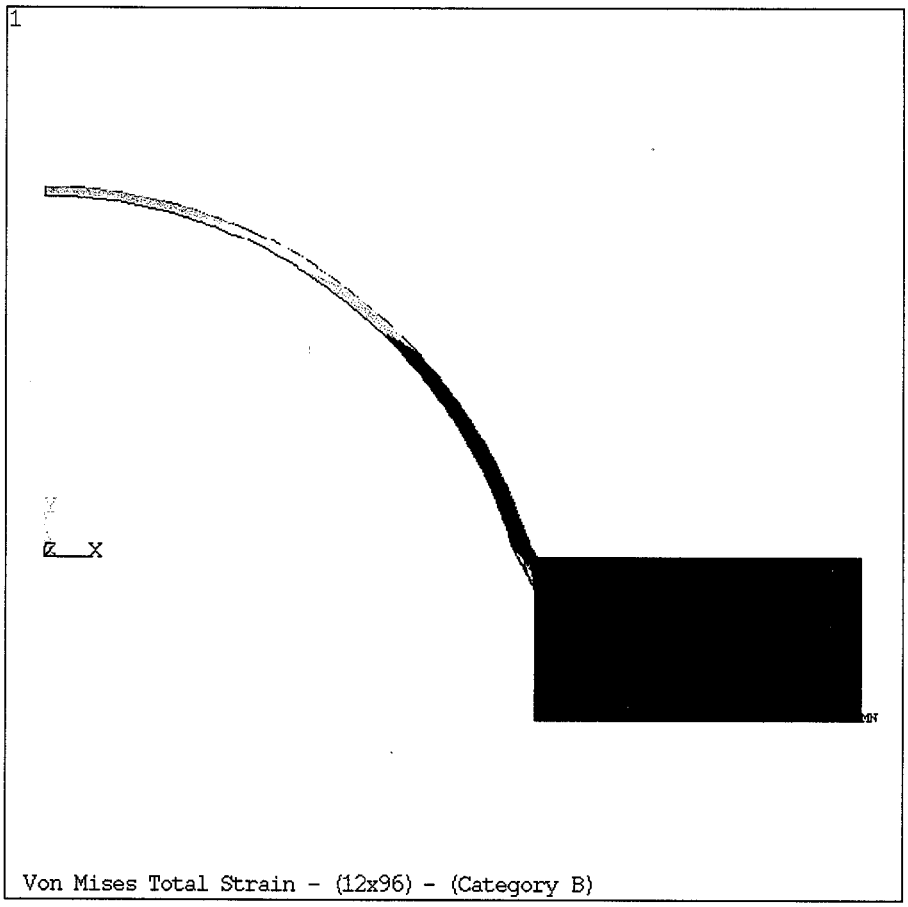

Figure 9 – Total Von Mises Strain Just Prior to Numeric Instability
Geometry-B – Axisymmetric (12 Elements)

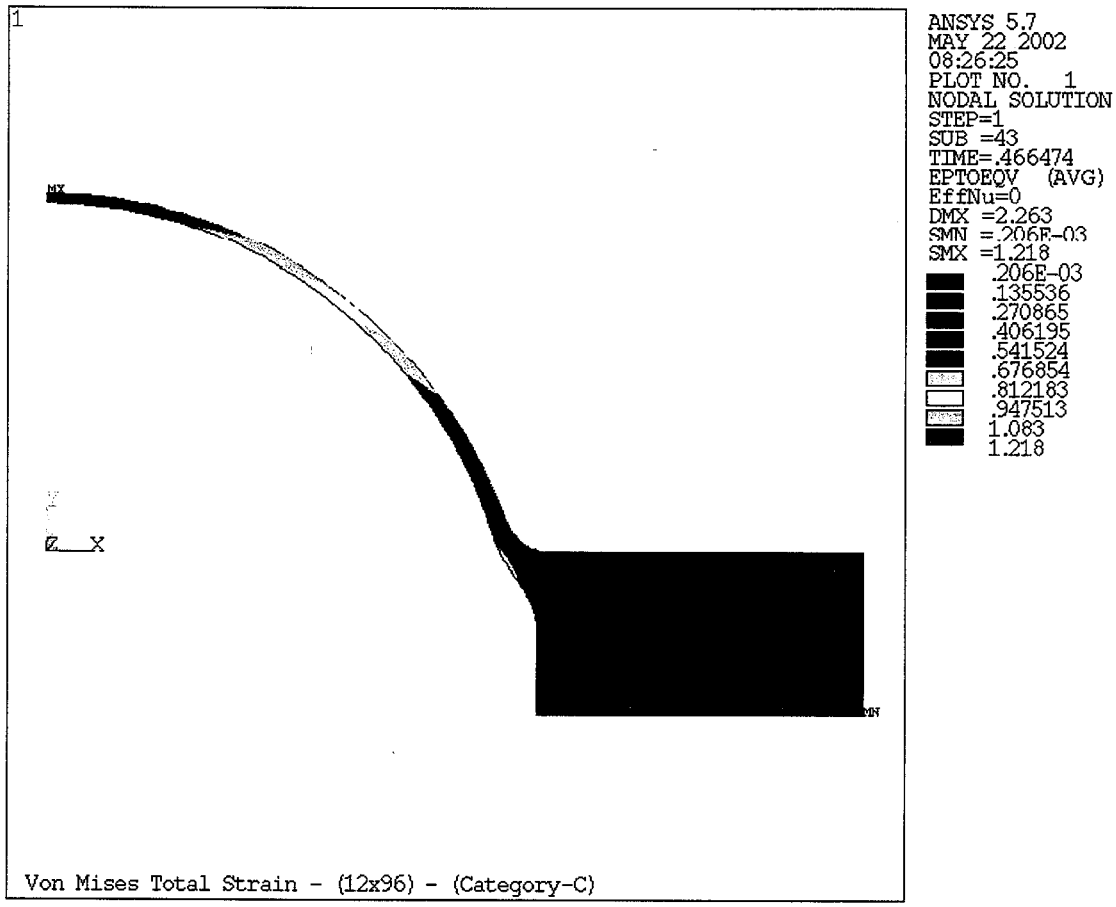

Figure 10 – Total Von Mises Strain Just Prior to Numeric Instability
Geometry-C – Axisymmetric (12 Elements)

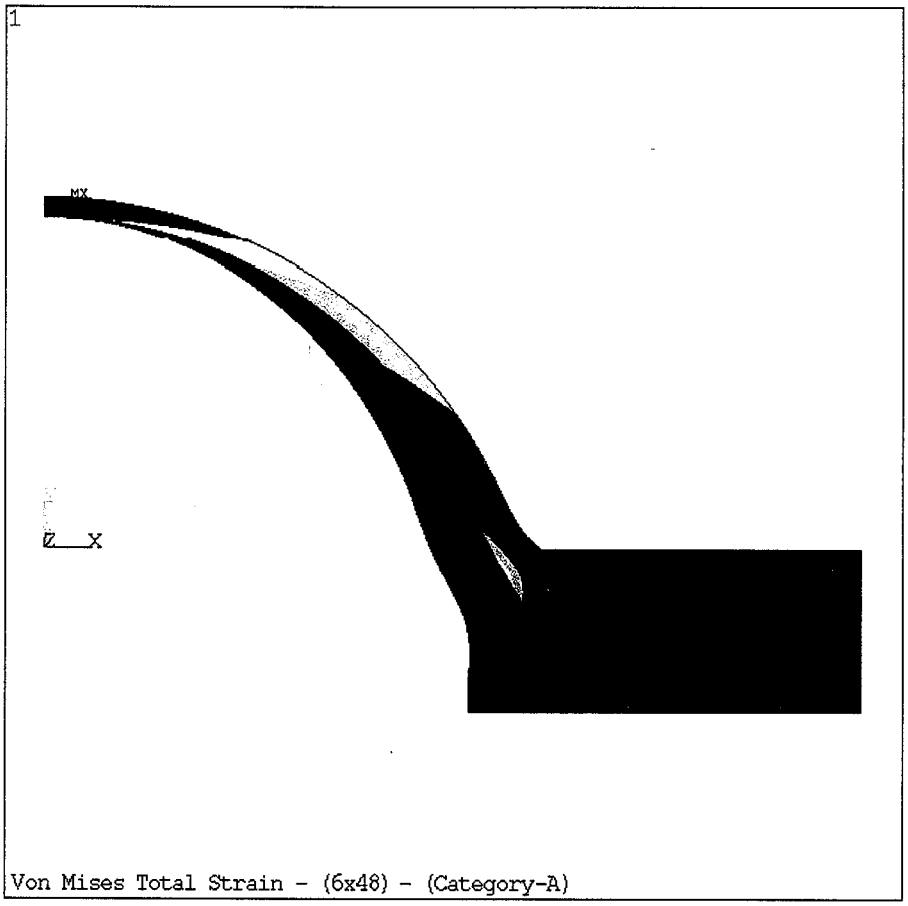

Figure 11 – Total Von Mises Strain Just Prior to Numeric Instability
Geometry-A – 3-Dimensional (6 Elements)

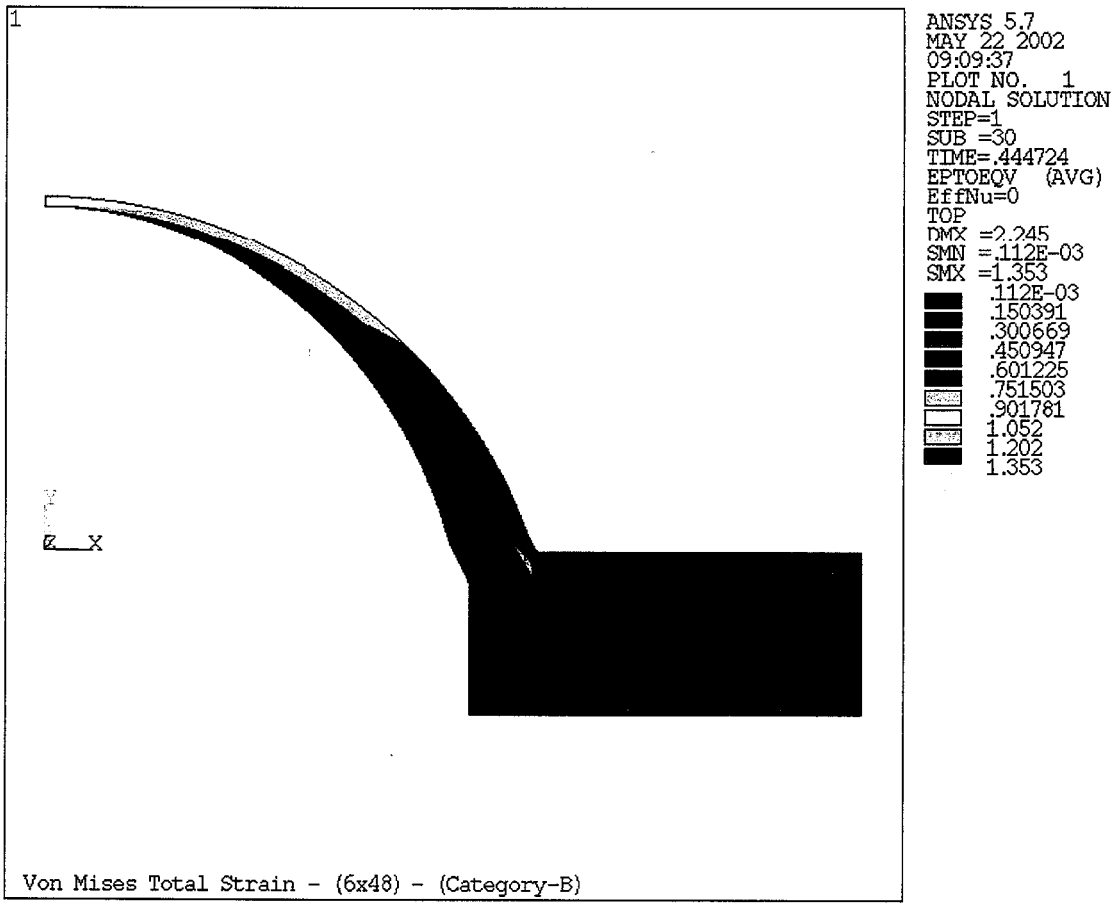

Figure 12 – Total Von Mises Strain Just Prior to Numeric Instability
Geometry-B – 3-Dimensional (6 Elements)

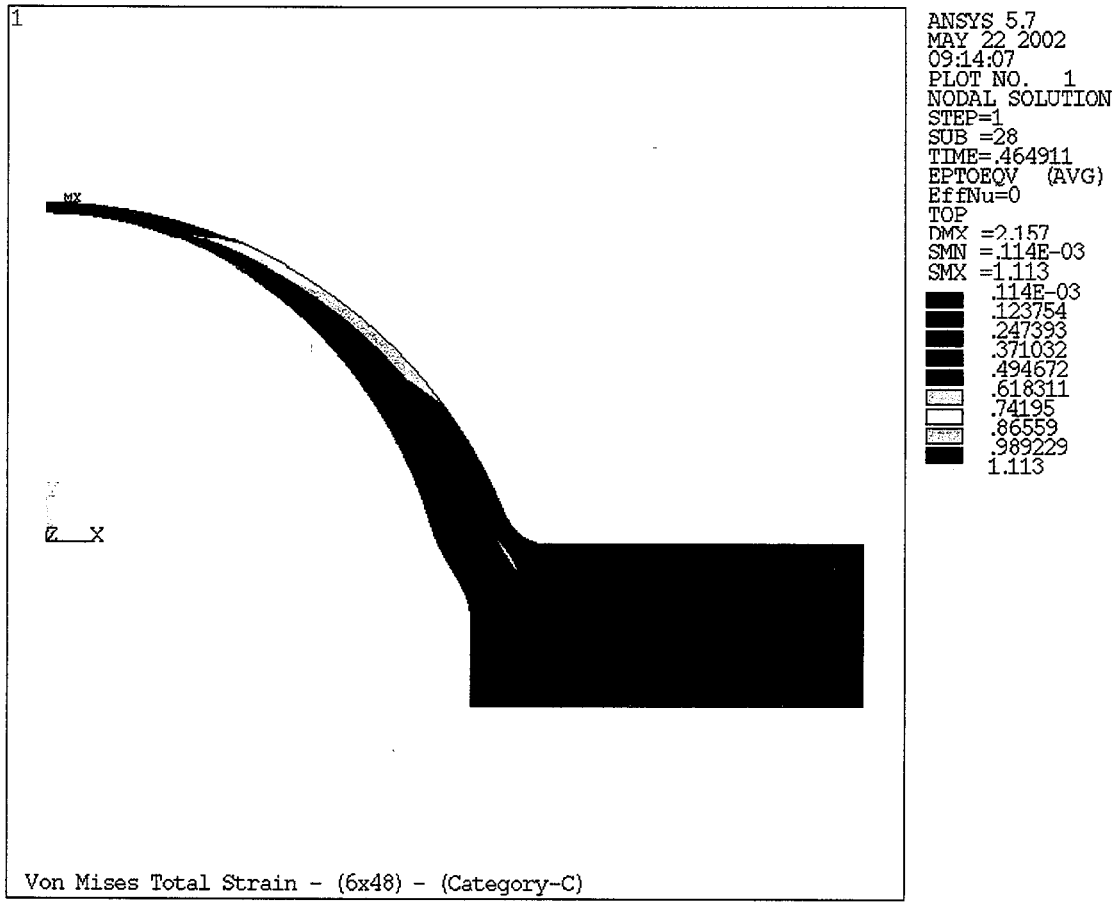

Figure 13 – Total Von Mises Strain Just Prior to Numeric Instability
Geometry-C – 3-Dimensional (6 Elements)

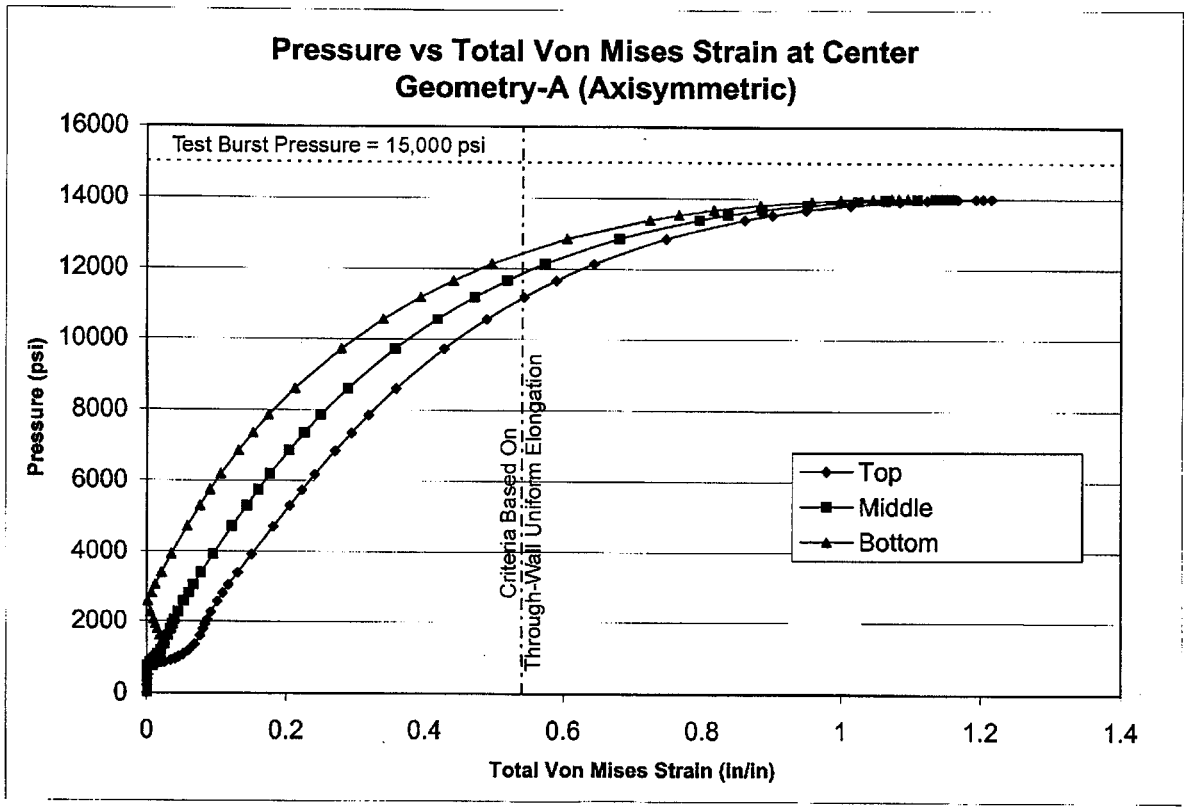

Figure 14 – Through-Wall Strain Results at Center of Disk
Geometry-A (Axisymmetric)

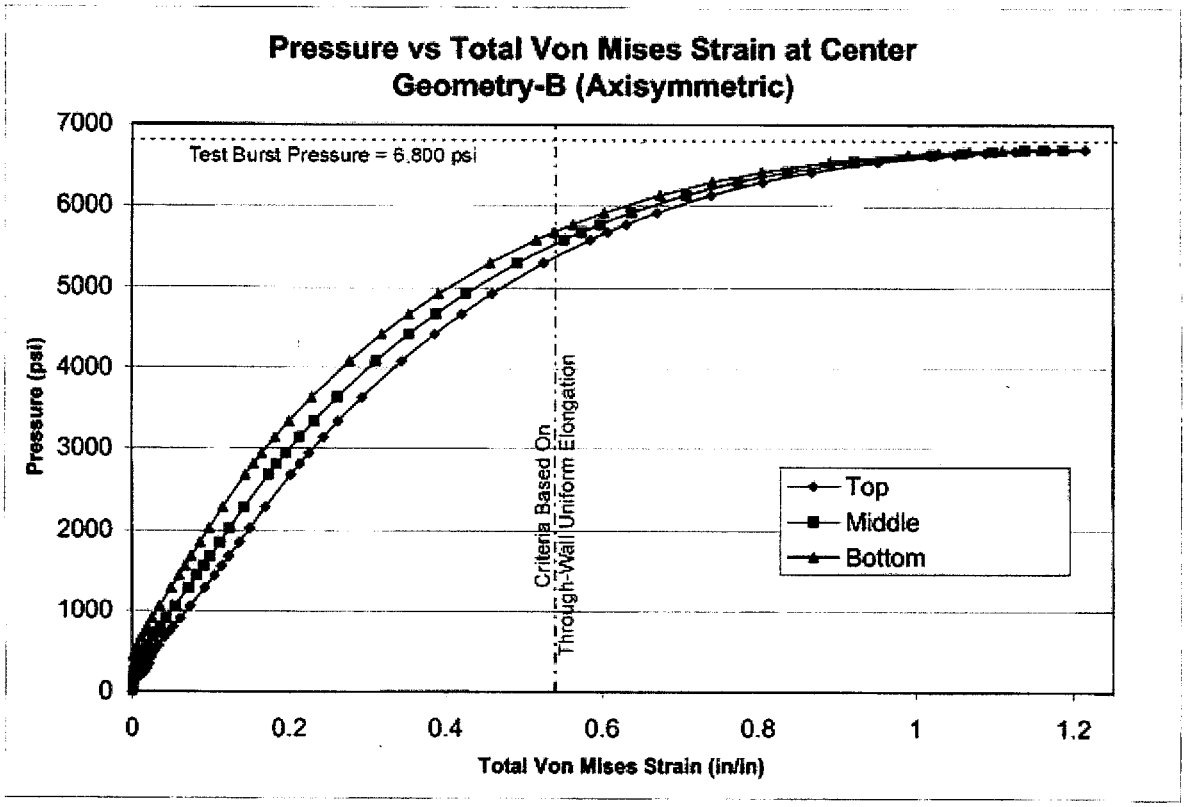

Figure 15 – Through-Wall Strain Results at Center of Disk
Geometry-B (Axisymmetric)

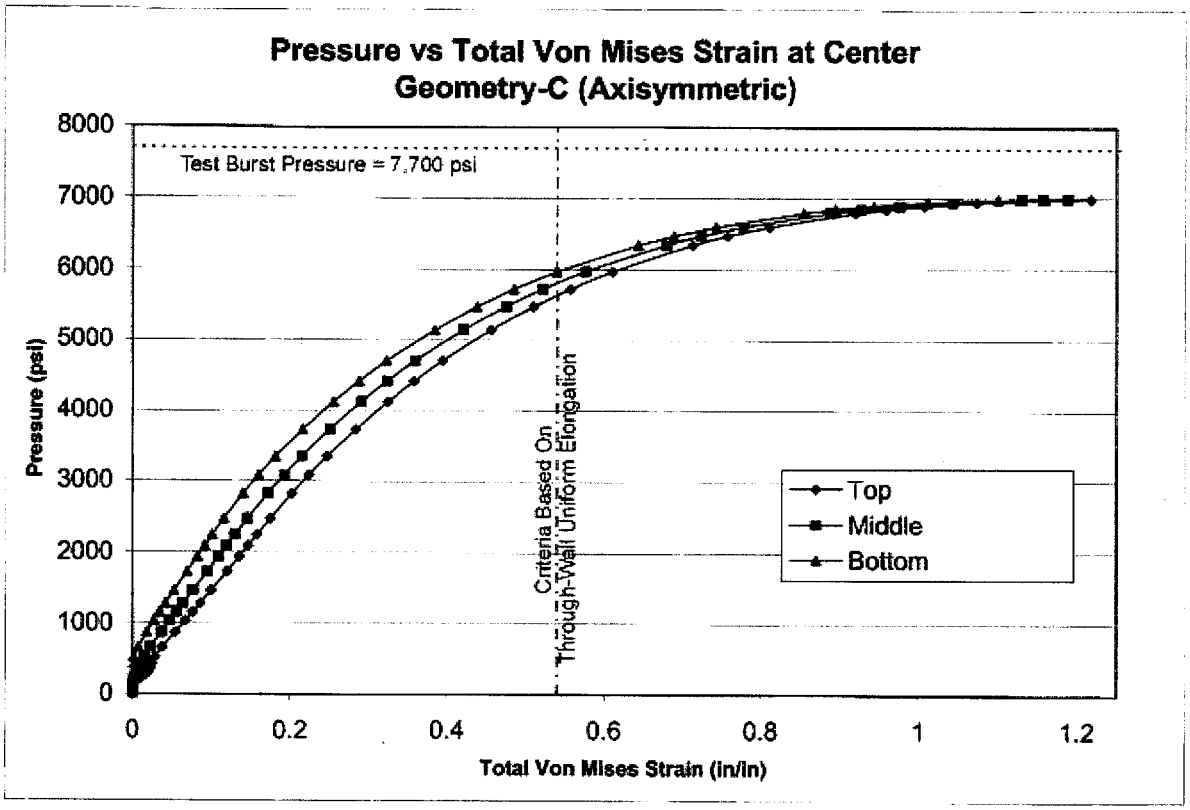

Figure 16 – Through-Wall Strain Results at Center of Disk
Geometry-C (Axisymmetric)

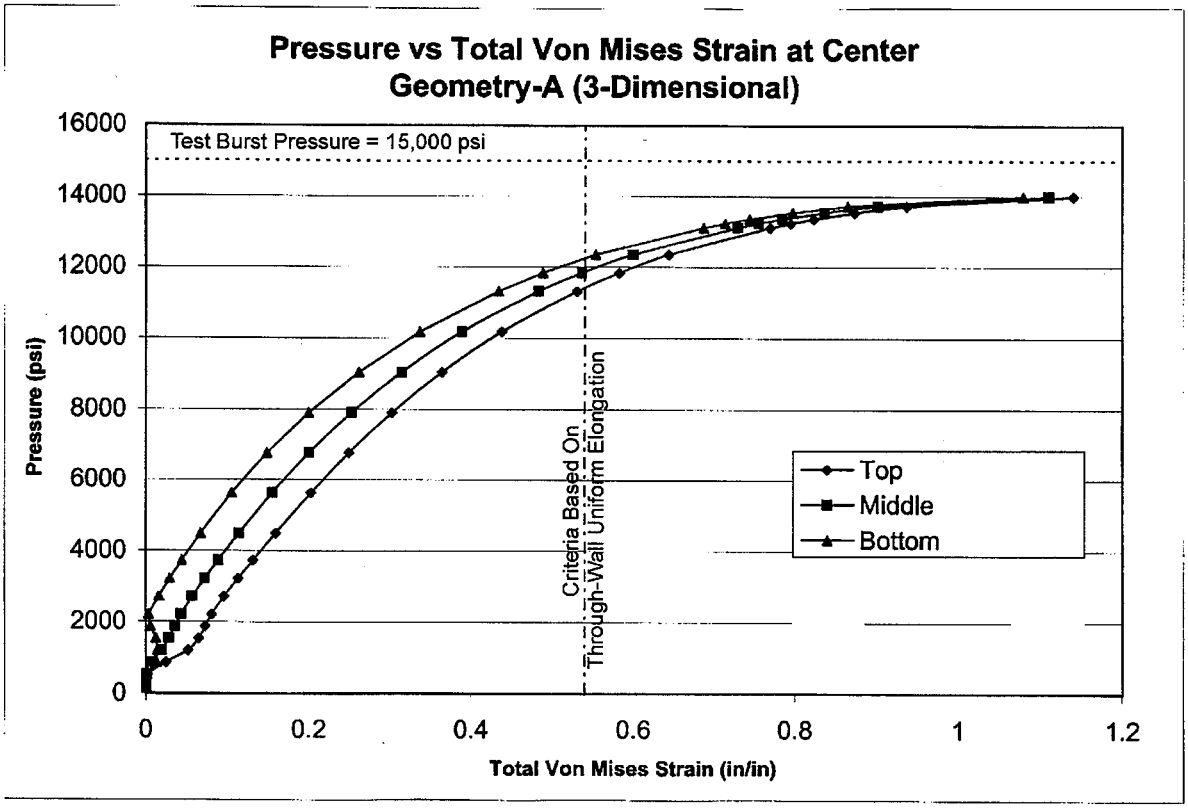

Figure 17 – Through-Wall Strain Results at Center of Disk
Geometry-A (3-Dimensional)

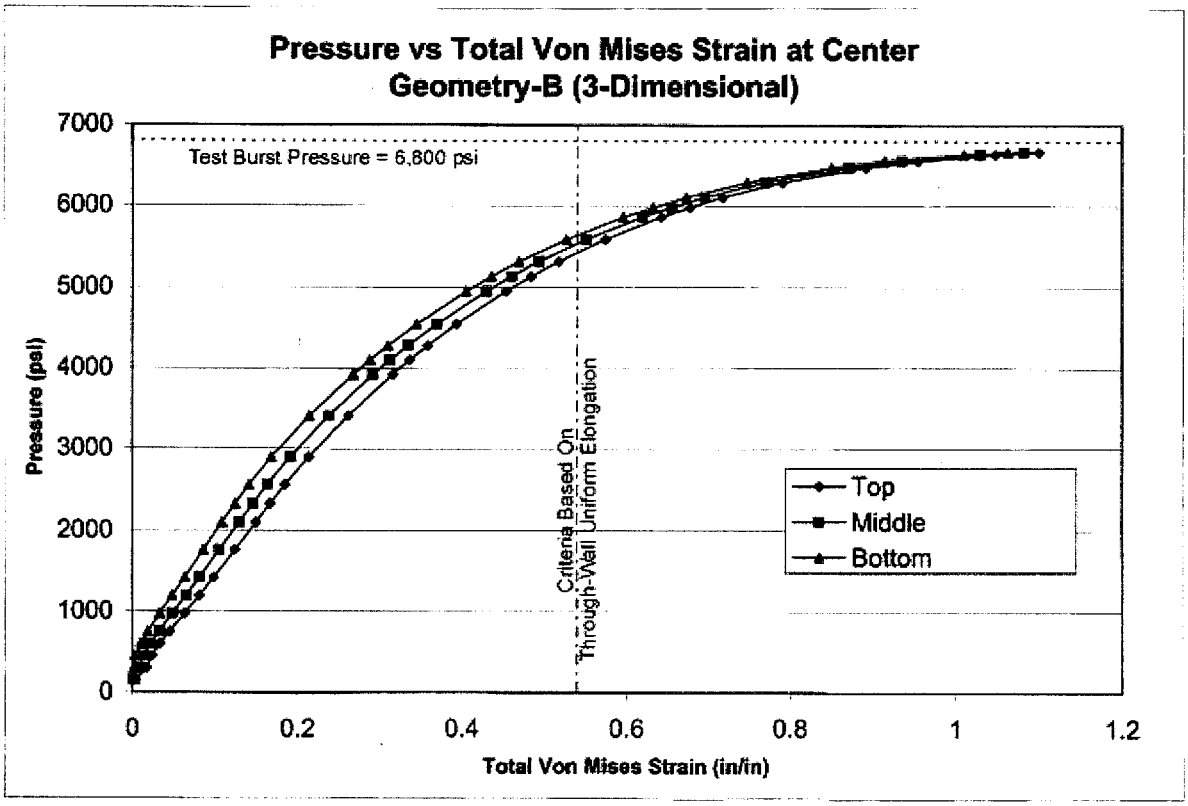

Figure 18 – Through-Wall Strain Results at Center of Disk
Geometry-B (3-Dimensional)

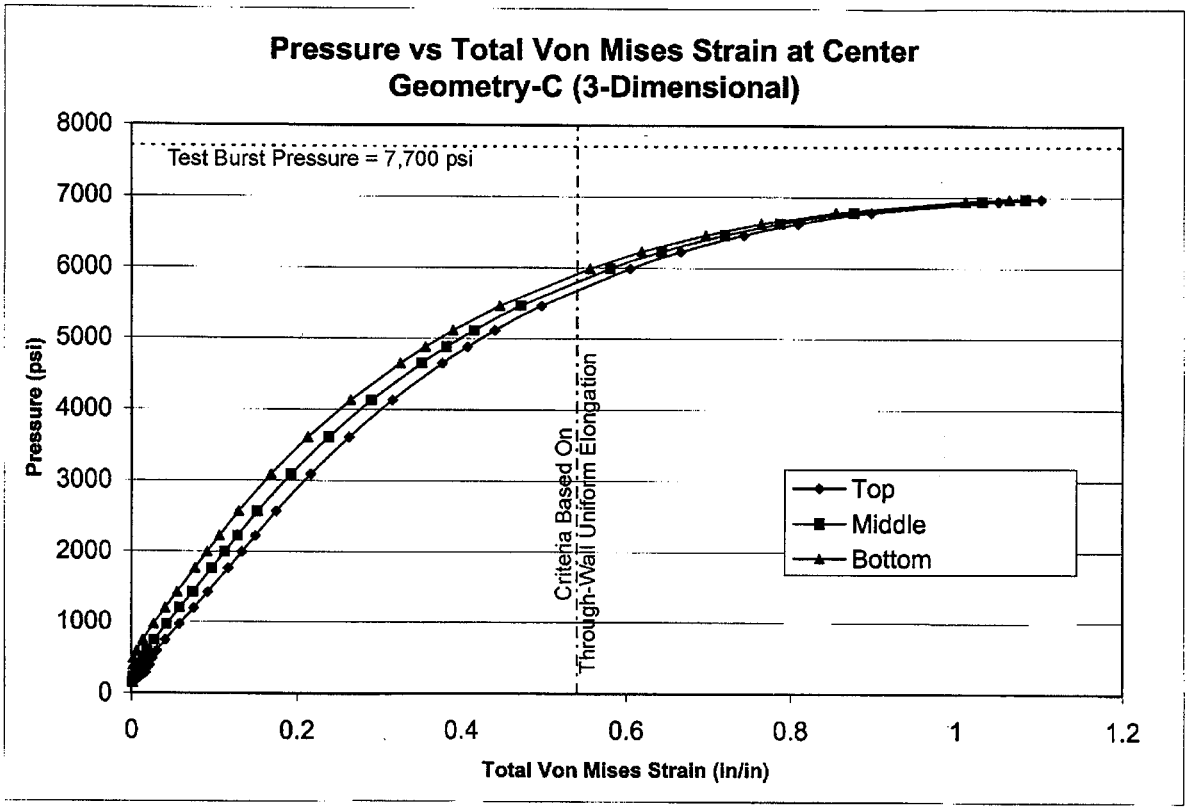

Figure 19 – Through-Wall Strain Results at Center of Disk
Geometry-C (3-Dimensional)

APPENDIX A

NRC Staff Comments and Questions on Davis-Besses Safety Significance Assessment (SIA-W-DB-01Q-301) Submitted April 8, 2002

NRC STAFF COMMENTS AND QUESTIONS ON DAVIS-BESSE SAFETY SIGNIFICANCE ASSESSMENT (SIA-W-DB-01Q-301) SUBMITTED APRIL 8, 2002

FAILURE CRITERION

(1) What is the technical basis of the failure criterion (e.g., strain exceeding 11.15%) used to determine the failure conditions of the cladding layer? Provide specific technical references in the literature that support the failure criterion used in this evaluation.

(2) How does the failure criterion (e.g., based on ultimate strain in a uniaxial tensile test) account for the effects of biaxial loading in the cladding, or triaxial loading in the cladding at the edges of the degradation cavity?

(3) The failure criterion applied in SIA report W-DB-01Q-301 (e.g., the minimum cross-sectional strain exceeding the failure strain of 11.15%) allows the strain levels in the cladding to exceed the critical strain value entirely through the thickness, leading to very large strains at the surface of the cladding, up to 49% in Table 5 of the SIA report. What is the technical basis for this approach, as opposed to the average cross-sectional strain, or the maximum cross-sectional strain?

(4) Did you explore a continuum damage mechanics analysis to give guidance of the failure criterion once the strains exceed the critical strain where necking/void growth starts? If not, provide the technical basis for not using a continuum damage mechanics analysis. [Poisson's ratio of 0.5 no longer applies once this critical strain level is exceeded, so the analysis is strictly not valid. (Poisson's ratio is continuously changing as the voids grow at the strains beyond the start of necking.) This results in a stress redistribution that is not accounted for in a standard elastic-plastic analysis.]

(5) How would the strain values change if the stress free temperature was assumed to be the stress relief temperature instead of 70°F, and the analysis accounted for the differential thermal expansion of the cladding and head steel at the operating temperature of 605°F?

GEOMETRY/MESHING

(A) Does the size of the degradation cavity and the transition from the cladding thickness to the head thickness that was used in the SIA report reflect current knowledge regarding the cavity geometry, in particular the undercut area described in Figure 13 on page 103 of the Davis-Besse Root Cause Analysis Report (CR2002-0891), dated April 15, 2002? What is the transition geometry assumed in the analyses?

(B) Is there sufficient mesh refinement through the cladding thickness to adequately capture the bending and shear strains at the edge of the cavity? Describe any sensitivity studies used to demonstrate the adequacy of the mesh refinement.

(C) Was the cladding deposited by weld wire? Do the thinner cladding thickness measurements from UT coincide with the locations of weld bead toes? In what direction do the cladding weld beads run relative to the long axis of the degradation cavity?

APPENDIX B

Pressure Vessels and Piping Division Paper No. 72-PVP-12, "Elasto-Plastic Analysis of Constrained Disk Burst Tests"

ted in U.S.A.

Paper No.
72-PVP-12

an ASME publication

P. C. RICCARDELLA

Materials and Stress Analysis,
Westinghouse Nuclear Energy Systems,
Pittsburgh, Pa.

Elasto-Plastic Analysis of Constrained Disk Burst Tests

The PVRC Subcommittee on Effective Utilization of Yield Strength has conducted an extensive series of pressurized burst tests on constrained disk specimens of seven steels. Elasto-plastic analyses have been performed for nine of these tests and the results are presented in this report. Good agreement between the analytical and experimental results all the way to failure pressure is illustrated by a comparison of centerline deflections. Interpretation of the analytical data indicates that both edge type and centerline type offailures are correlated reasonably well by the conventional reduction in area from a uniaxial tensile test once triaxiality is accounted for.

Introduction

THE PVRC Subcommittee on Effective Utilization of Yield Strength has conducted a series of constrained disk burst tests [1][1] using the disk specimen and test setup illustrated in Fig. 1. In order to interpret these tests and their relation to the safety margins which exist in the components of a Westinghouse nuclear steam supply system, elasto-plastic analyses have been performed on three disk geometries with three materials each. The three materials considered were type 304 stainless steel, ASTM A533B low-alloy steel, and ABS-C carbon steel. These materials are representative of reactor core support structures and piping, the reactor pressure vessel, and plant component supports, respectively. A summary of the mechanical properties from uniaxial tensile tests performed on the actual disk materials is given in Table 1.

Extensive data from the disk tests, including burst pressures and experimental pressure versus deflection curves have been reported in references [1] and [2]. Some of the disks failed at the disk centerlines, while others failed along the edge of the disks at the fillet between the thin and thick regions. Table 2 summarizes the failure data for the disks considered in this analysis, which include three centerline failures and six edge failures. The details of the three disk geometries are tabulated in Fig. 1.

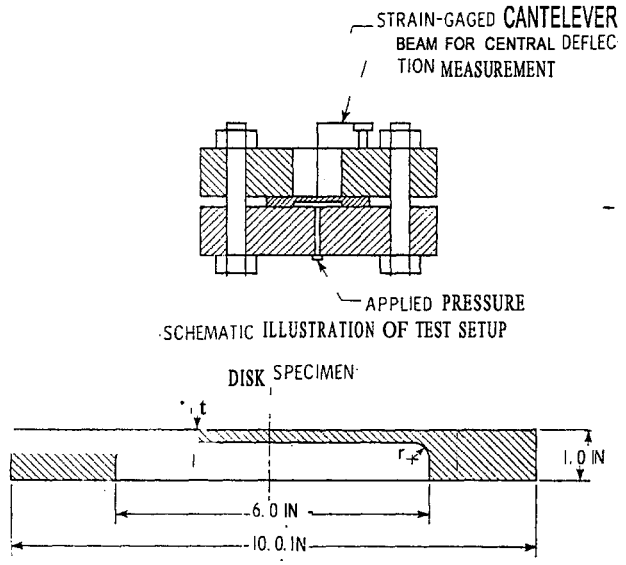

GEOMETRY	THICKNESS (t)	FILLET RADIUS (r)
A	0.25 IN	0.375 IN
B	0.125 IN	0.125 IN
C	0.125 IN	0.375 IN

Fig. 1 PVRC disk fest details

[1] Numbers in brackets designate References at end of paper.

Contributed by the Pressure Vessels and Piping Division for presentation at the Petroleum Mechanical Engineering Conference with Pressure Vessels and Piping Conference, New Orleans, La., September 17-21, 1972, of THE AMERICAN SOCIETY OF MECHANICAL ENGINEERS. Manuscript received at ASME Headquarters, June 6, 1972. Paper No. 72-PVP-12.

Copies will be available until June, 1973.

Discussion on this paper will be accepted at ASME Headquarters until October 23, 1972

Table 1 Material properties

Material	.2" Y.S. (PSI)	$S_{ult.}$ (PSI)	$\epsilon_{ult.}$ (In/In)	Reduction in area	A* (PSI)	n*
Type 304 Stainless Steel	34,000.	84,000.	.54	.74	193,060.	.494
A-533B LowAlloy Steel	74,000.	96,000.	.17	.68	146,000.	.141
ABS-C Carbon Steel	39,000.	64,000.	.31	...66	115,130.	.242

* Stress-strain curve assumed to be of form $\sigma = A\,\epsilon^n$

Table 2 Experimental failure data

Material	Geometry	Burst Pressure (PSI)	Type of Failure
304 S.S.	A	15,000.	Edge
	B	6,800.	Center
	C	7,700.	Center
A-S33 B	A	11,000.	Edge
	B	5,300.	Edge
	C	6,700.	Center
ABS-C	A	9,800.	Edge
	B	3,750.	Edge
	C	4,940.	Edge

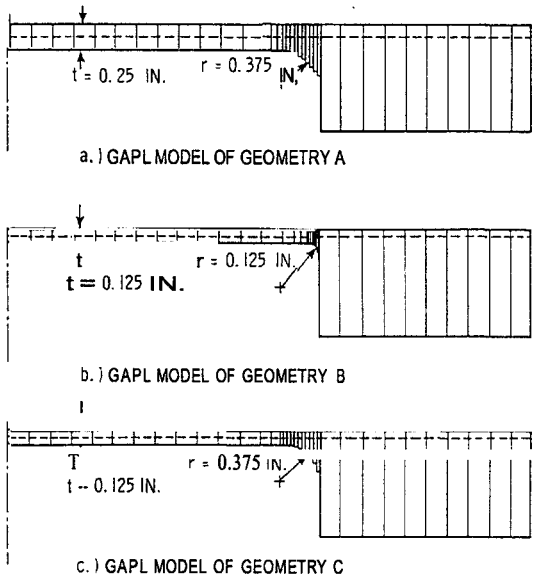

Fig. 2 Computer models of PVRC disks

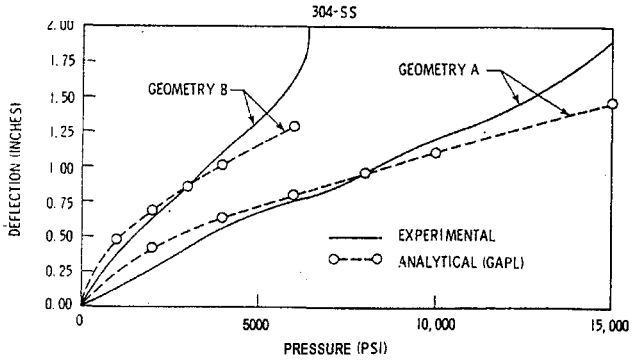

Fig. 3(a) PVRC disk tests—centerline deflection versus pressure (experimental and analytical results for 304 stainless steel disks)

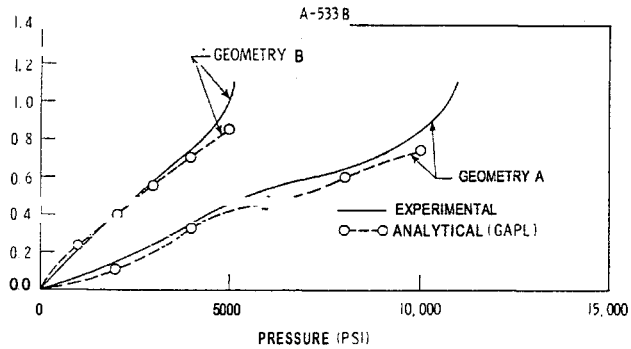

Fig. 3(b) PVRC disk tests—centerline deflection versus pressure (experimental and analytical results for A-533 B low alloy steel disks)

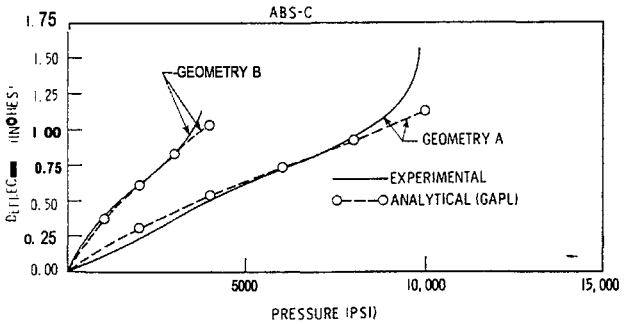

Fig. 3(c) PVRC disk tests—centerline deflection versus pressure (experimental and analytical results for ABS-C carbon steel disks)

Fig. 3

Analysis

The analysis of the disks was performed using the computer program GAPL-3 [3]. This program performs elasto-plastic, large-deformation analysis for stresses, strains, loads, and deflections of thin plates or axially symmetric shells with pressure loading and deflection restraints. The discrete element method employed in GAPL-3 requires fewer elements than conventional finite element techniques to adequately describe structures with high stress gradients because it makes use of a two-layered system of elements: one layer for the strain-displacement field, and a second layer for the stress field. The body is first divided into constant thickness, finite length strain-displacement elements along the axis of the body. The deflections in the elements are represented by a bending type polynomial along the axis and by a linear variation through the thickness. Each element is then further subdivided into constant stress regions in which the stresses are found as a function of the strains in the region. It is the deflection elements, however, which dictate the size of the problem.

The pressure loading is applied in steps and an equilibrium solution is found at each step by iterating for both geometric and material nonlinearities. The choice of incremental or deformation theory of plasticity is made by the user according to the size of the load steps he chooses. Since the program must iterate at each load step, the finer the load steps, the more costly the problem becomes.

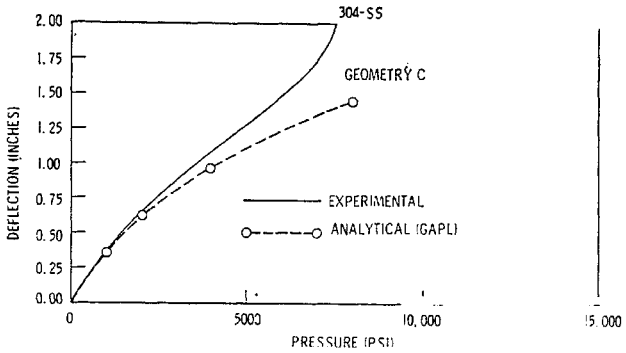

Fig. 4(a) PVRC disk tests—centerline deflection versus pressure (experimental and analytical results for 304 stainless steel disks)

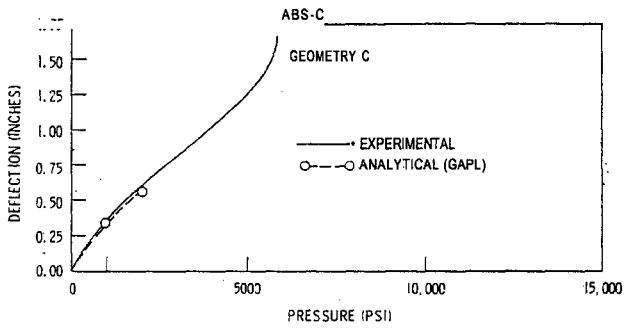

Fig. 4(c) PVRC disk tests—centerline deflection versus pressure (experimental and analytical results for ABS-C carbon steel disks)

Fig. 4

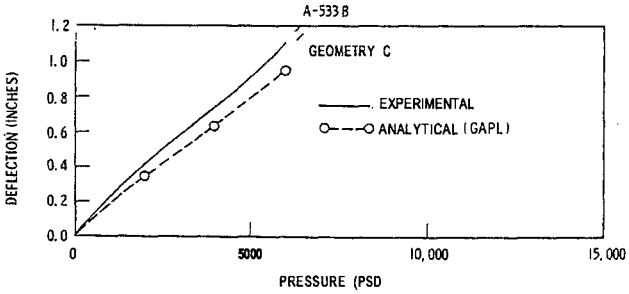

Fig. 4(b) PVRC disk tests—centerline deflection versus pressure (experimental and analytical results for A-533 B low alloy steel disks)

Table 3 Strain concentration factors

Material	Exponent (n)	K_ϵ (1/n)	GAPL RESULTS Geometry A K_{GAPL}	Geometry A K_ϵ/K_{GAPL}	Geometry B K_{GAPL}	Geometry B K_ϵ/K_{GAPL}	Geometry C K_{GAPL}	Geometry C K_ϵ/K_{GAPL}
A-533 B	.141	7.1	7.2	.98	7.5	.94	8.2	.86
ABS-C	.242	4.1	5.3	.77	6.1	.68	6.6	.62
304-SS	.494	2.0	3.6	.56	4.5	.45	5.2	.38

The three PVRC disk geometries were represented by the discrete strain-displacement element models shown in Fig. 2 In the thin portion of the disks eight stress regions were specified for each strain-displacement element, while in the filet regions twelve stress regions per element were used. Material properties for the three steels analyzed were input in terms of a power hardening law, using the constants A and n listed in Table 1. Both fine and crude load steps were tested to evaluate the effect of deformation versus incremental theories of plasticity, and the results were practically identical which indicates that the problem is a proportional loading situation. The production runs were then made using five load steps per case so that a reasonable representation of stresses and displacements as a function of applied pressure could be obtained.

Results

A comparison of the experimental and analytical centerline deflections at various pressures is given for geometries A and B in Fig. 3 and for geometry C in Fig. 4. The agreement is excellent all the way to failure pressure in eight of the nine cases considered. In the ninth case (ABS-C, geometry C) some difficulty was experienced in getting convergence at high pressures, although the experimental-analytical agreement was good at low pressures. In all cases the experimental data shows a tailing up as the pressure approaches burst pressure which the analytical results fail to predict. Since the GAPL program does not account for reduction in thickness, it can not be expected to predict tensile instability which the experimental tailing up represents.

Since the analytical prediction of. centerline deflection was so good, it is expected that the stress and strain distributions predicted by GAPL are reasonable estimates of what occurred in the actual test specimens. Some reservation is called for in the fillet region, however, since the thin shell approximations of the GAPL program are not strictly valid there. The GAPL analysis includes plastic hinge type of strain redistribution, but the strain concentration effect due to fillet radius is not accounted for since the predicted strain distribution in the cross section of the fillet is linear there by ass tion.

As the ire increased, the computed stresses at the disk centerlines approached a state of uniform biaxial membrane stress with n bendi stress. In the fillet, the membrane stresses were lower than at the disk centerline, but the stresses on the inside surface of the fillet were the highest in the disk 6, and 7 summarize the computed stress and strain data for the fillet and centerline regions of the disks for the 304 SS, the A-533 B and the ABS-C, respectively The curves give maximum valhes of von Mises equivalent stress and strain in the two locations.

Several authors [6] have noted that the strain concentration (or redistribution) in the fillet in tests such as this should increase as the strain hardening exponent (n) decreases. As a first approximation, use of a strain concentration factor (K_ϵ) which is inversely proportional to n has been suggested [7]. In Fig. 8, the maximum radial fillet strains from the GAPL analysis have been cross-plotted against centerline deflections from Figs. 3 and 4 in order to study the effect of hardening exponent upon strain redistribution. The trend of increasing strain concentration with decreasing strain hardening is evident in this figure for all three geometries.

A simple elastic analysis has been performed on the disks in order to test the simple inverse proportion rule mentioned previously. The resulting maximum stresses in the fillet have been divided by Young's modulus and the results are given by the elastic lines in Fig. 8. Strain concentration factors have been computed at three discrete values of centerline deflection (0.6 in., 0.8 in., and 1.0 in.) by dividing the strains from the elasto-plastic GAPL analysis by the elastically computed strains at each deflection. The resulting strain concentration factors were then averaged over the three deflections, and these average values are listed in Table 3. This table shows that while the $(1/n)$ approximation is quite good for the lowest strain hardening exponent (n = 0.141), it tends to get worse as n increases. The inverse

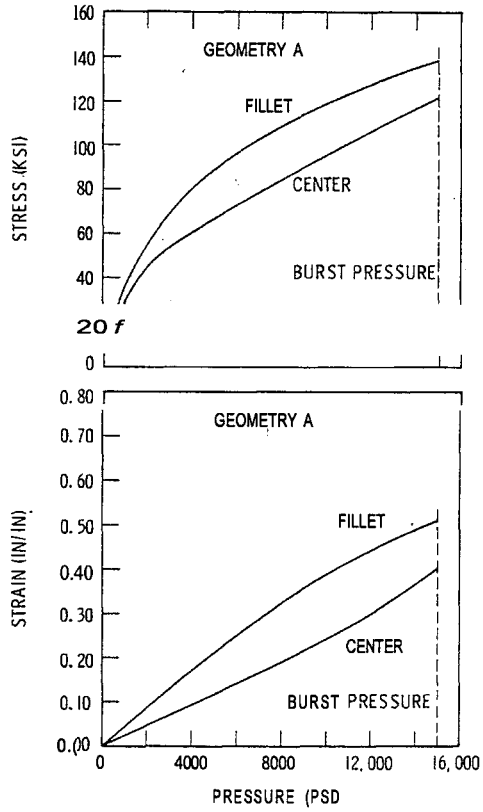

Fig. 5(a) Sfress and strain data for 304 stainless steel disks

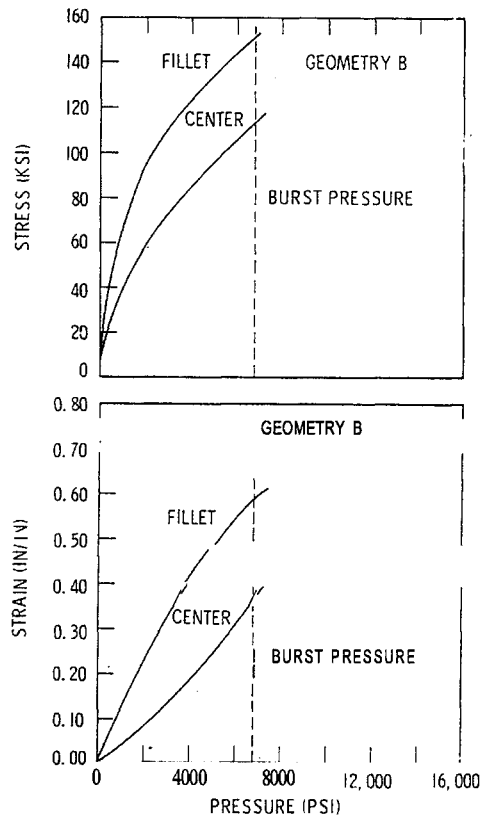

Fig. 5(b) Stress and strain data for 304 stainless steel disks

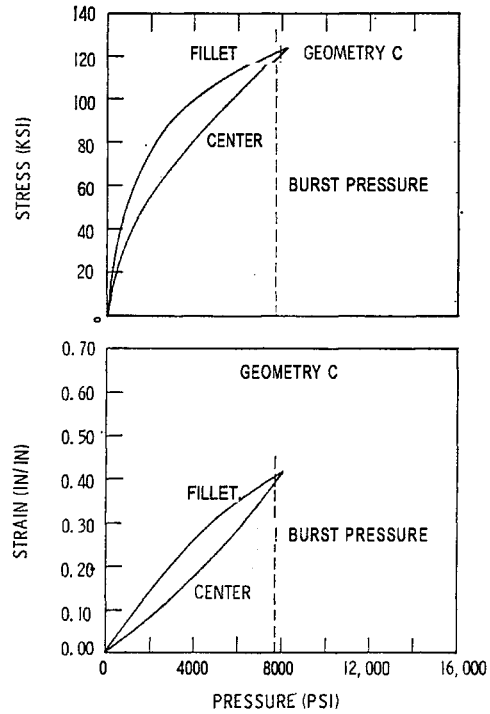

Fig. 5(c) Stress and strain data for 304 stainless steel disks

Fig. 5

proportion rule substantially underestimates the strain concentration for the stainless steel disks ($n = 0.494$).

Interpretation of Results

An interesting interpretation of this work arises when the equivalent strain levels at failure shown in Figs. 5, 6, and 7 are tabulated. All of the edge failures occurred at approximately the same strain level (~50 percent) and all of the centerline failures occurred at approximately the same strain level (~35 percent). (See Table 4). This seems surprising at first, since the ultimate or uniform strains for the three materials are 54 percent for the stainless steel, 17 percent for the low alloy steel, and 31 percent for the carbon steel as indicated in Table 1. However, the ultimate or uniform strain in a tensile test is somewhat artificial as a material property since it is really a measure of incipient tensile instability, and as such is geometry dependent.

Inspection of the material data in Table 1 indicates that the only tensile property which is approximately constant for all three materials is the reduction in area (R.A.). This suggests that reduction in area might be a good property for correlation of the test data. Before doing so, however, it is convenient to introduce the concept of triaxiality factor *(TF)* [8].

$$TF = 3\sigma_{mean}/\sigma_{eq}$$

$$\sigma_{mean} = \frac{(\sigma_1 + \sigma_2 + \sigma_3)}{3} \tag{1}$$

$$\sigma_{eq} = \frac{1}{\sqrt{2}}[(\sigma_1 - \sigma_2)^2 + (\sigma_2 - \sigma_3)^2 + (\sigma_3 - \sigma_1)^2]^{1/2}$$

$\sigma_1, \sigma_2, \sigma_3$ = principal stresses

Note that for uniaxial tension $TF = 1$, for pure biaxial tension $TF = 2$, and for pure triaxial tension $TF = \infty$.

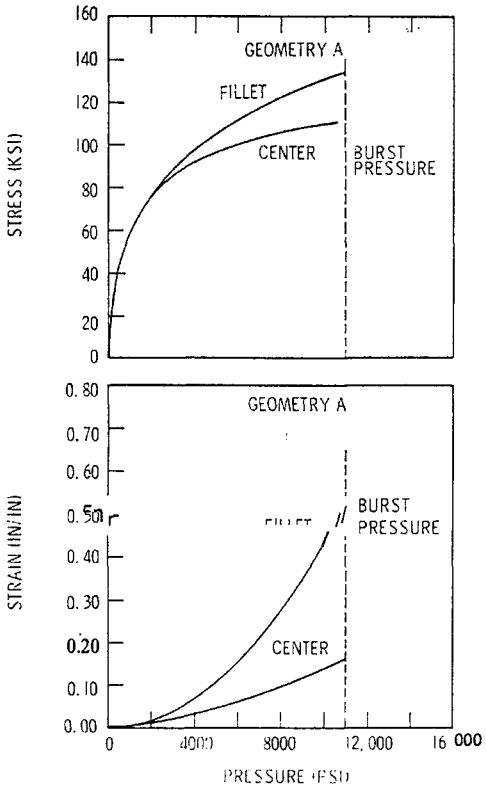

Fig. 6(a) Stress and strain data For A-533 B low alloy steel disks

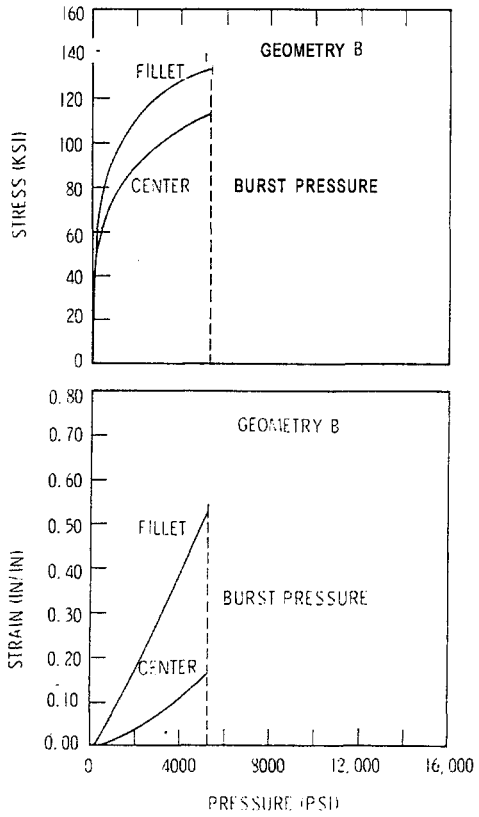

Fig. 6(b) Stress and strain data for A-533 B low alloy steel disks

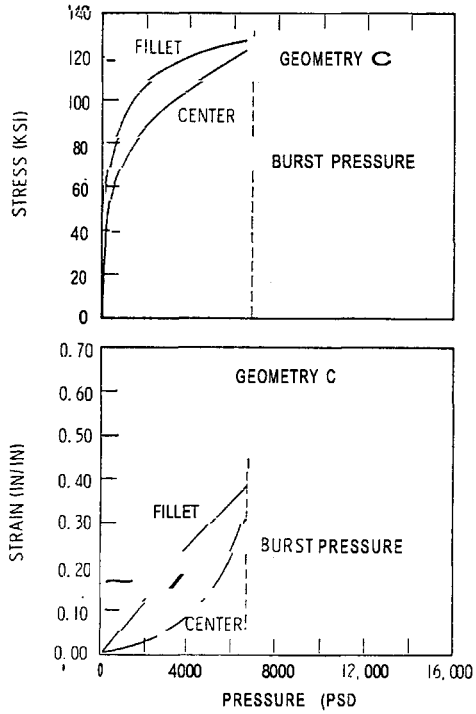

Fig. 6(c) Stress and strain data for A-533 B low alloy steel disks

Fig. 6

Generally, the amount of strain that a material can withstand before fracture is expected to decrease with increasing triaxiality of the imposed stress state. Davis and Connelly [8] have suggested that the triaxiality factor as defined previously might be an effective parameter with which to study the reduction in ductility due to multiaxial state of stress. That is:

$$\epsilon_{\substack{\text{crit} \\ \text{multiaxial}}} = \epsilon_{\substack{\text{crit} \\ \text{uniaxial}}} Xf(TF) \tag{2}$$

Where $f(TF)$ is a monotonically decreasing function.

Investigation of failure data from several sources [9, 10, 11, 12] indicates that, in the absence of severe anisotropy, the following expression is not a bad first approximation of the influence of triaxiality upon ductility:

$$f(TF) = 1/TF \tag{3}$$

The triaxiality factors for the disk tests at failure were 2.0 for the centerline region and about 1.65 for the fillet based upon the computed stresses in those regions. The tensile tests used to measure reduction in area can be assumed to have had a triaxiality factor of 1.0. In addition, the tensile tests were performed for both longitudinal and transverse tensile specimens indicating very little anisotropy in the disk materials, so that the approximation of equation [3] should apply. Thus, as a first approximation of multiaxial ductility, the reduction in area values for the three materials have been divided by the appropriate triaxiality factors and listed in Table 4. The final column of Table 4 lists the ratios of equivalent strain in the failure location to the multiaxial ductility at that location. The correlation is always better than 30 percent, and the average error is about 16 percent.

Casting this same information in a slightly different format, the question of how well the foregoing scheme predicts failure pressure can be answered. Using the postulate that failure occurs whenever the value of equivalent strain exceeds the re-

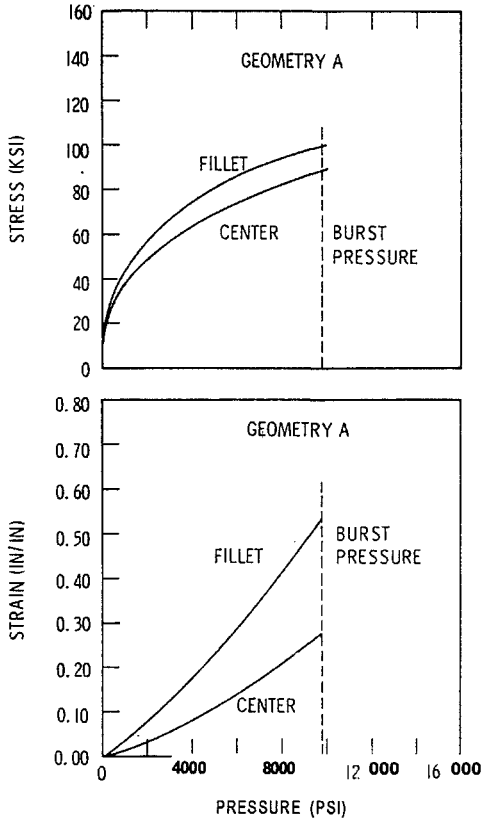

Fig. 7(a) Stress and strain data for ABS-C carbon steel disks

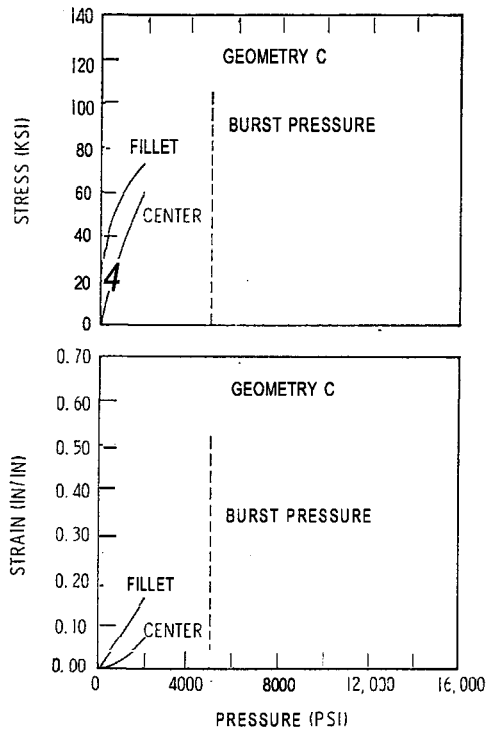

Fig. 7(c) Stress and strain data for ABS-C carbon steel disks

Fig. 7

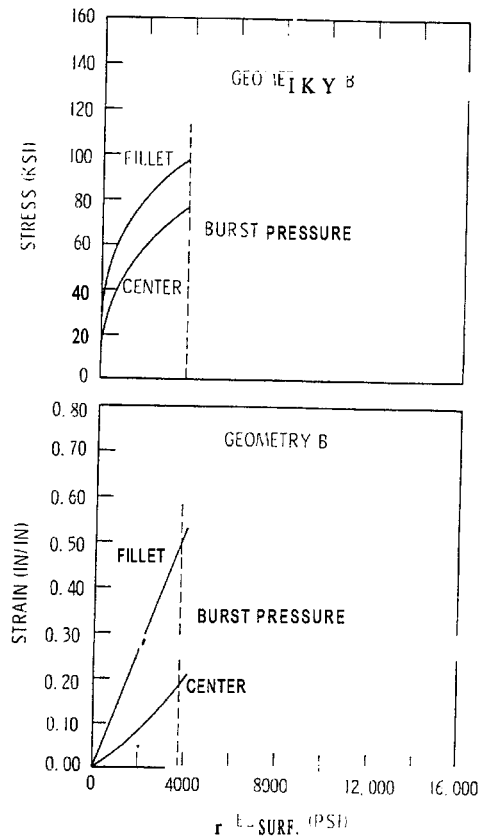

Fig. 7(b) Stress and strain data for ABS-C carbon steel disks

duction in area divided by the triaxiality ratio (multiaxial ductility) at any point in the disk, burst pressures as well as failure locations can be predicted from the analytical strain versus pressure curves of Figs. 5, 6, and 7. Table 5 presents such predictions for the test cases considered here. The predicted burst pressures give reasonably accurate estimates of the actual burst pressures, and the predicted location of failure was correct in all cases but one (304 S.S.—geometry B).

Summary and Conclusions

Results of an elasto-plastic, finite-deformation analysis of selected PVRC disk tests are presented and, in general, there is good agreement between experiment and analysis, which is illustrated by a comparison of the predicted and actual deflections at the disk centerlines as a function of applied pressure. A definite trend of increasing strain concentration in the fillet of the disks as the strain hardening decreases is apparent in the data for all three geometries analyzed. The order of magnitude of this trend supports the assumption of Section 3 of the ASME Boiler and Pressure Vessel Code that plastic strain concentration is inversely proportional to the strain hardening exponent, at least for low values of this exponent.

A scheme for predicting burst pressure from the analytical stress and strain data using the reduction in area from a conventional uniaxial tensile test as a critical strain parameter is suggested. Failure is posited when the computed equivalent strain in the disks exceeds the reduction in area property of the material adjusted by the triaxiality of the stress state. The scheme is shown to be reasonably consistent for the limited number of cases considered.

This analysis demonstrates that it is possible to predict failure loads for material and hardware similar to those used in commercial nuclear power plants, provided that a reasonably accurate

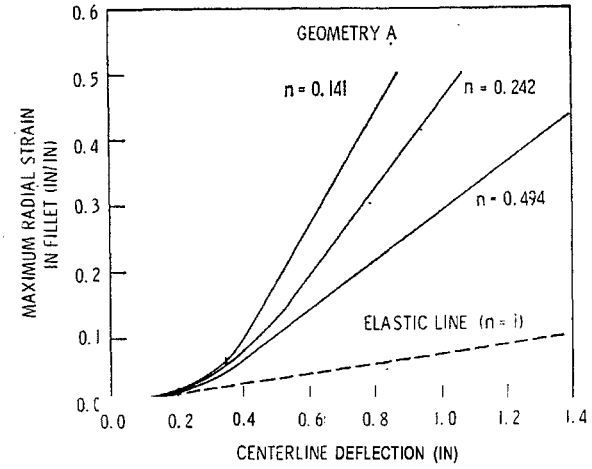

Fig. 8(a) Strain concentration in fillet for various strain hardening exponents

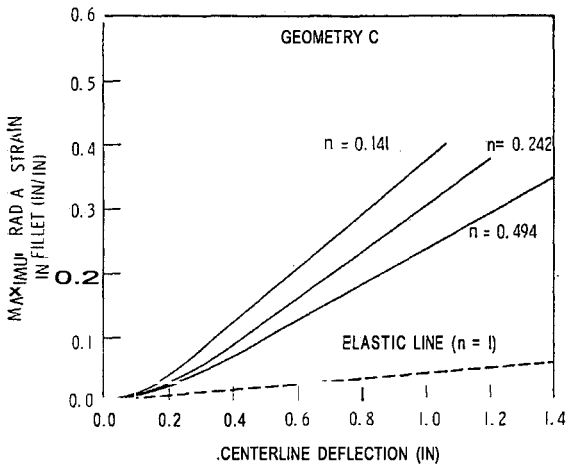

Fig. 8(c) Strain concentration in fillet for various strain hardening exponents

Fig. 8

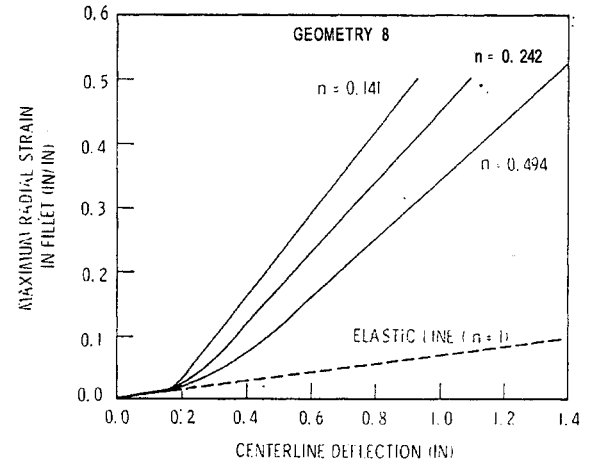

Fig. 8(b) Strain concentration in fillet for various strain hardening exponents

elasto-plastic analysis can be performed. Extension of such an analysis to the more complex loading and geometric conditions which exist in actual plant components will allow accurate evaluations of the margins of safety which exist in these components.

Acknowledgments

The author would like to thank Mr. G. A. Spiering of Teledyne Materials Research Company for his help in interpreting the test data and Dr. A. L. Thurman of Westinghouse Bettis Atomic Power Laboratory for the use of his computer program, without which the analysis could not have been performed.

References

1 Cooper, W. E., Kottcamp, E. H., and Spiering, G. A., "Experimental Effort on Bursting of Constrained Disks as Related to the Effective Utilization of Yield Strength," ASME, 71-PVP-49, May 1971.

2 *P.V.R.C. Subcommittee on Effective Utilization of Yield Strength Experimental Report of Pilot Program and Phase II Effort on Bursting of Constrained Discs,* Teledyne Materials Research Co., Technical Report No. E-1178(b).

3 Thurman, A. L., *GAPL-3-A Computer Program for the Inelastic Large Deflection Stress Analysis of a Thin Plate or Axially Symmetric Shell With Pressure Loading and Deflection Restraints,* WAPD-TM-791, Bettis Atomic Power Laboratory, Pittsburgh, Pa., June 1969.

4 Radomski, M., and White, D. J., "Some Theoretical Considerations Relating to Strain Concentration in Elasto-Plastic Bending of Beams," *Journal of Strain Analysis,* Vol. 3, No. 4, 1968, pp. 304-312.

5 White, D. J., and Radomski, M, "Strain Concentration in Beams Under Cyclic Plastic Straining," *Journal of Strain Analysis,* Vol. 3, No. 4, 1968, pp. 313-324.

Table 4 Computed strains at failure

Material	Geometry	Type of Failure	CENTERLINE DATA: Strain At Failure	Triaxiality Factor (TF)	Multiaxial Ductility ($\frac{\bar{\varepsilon}_f}{TF}$)	EDGE DATA: Strain At Failure	Triaxiality Factor (TF)	Multiaxial Ductility ($\frac{\bar{\varepsilon}_f}{TF}$)	RATIOS: Failure Strain / Ductility
304 S.S.	A	Edge	.40	2.0	.37	.51	1.63	.45	1.12
	B	Center	.37	2.0	.37	.58	1.65	.45	1.0
	C	Center	.39	2.0	.37	.41	1.65	.45	1.05
A-533 B	A	Edge	.16	2.0	.34	.52	1.67	.41	1.27
	B	Edge	.17	2.0	.34	.53	1.67	.41	1.29
	C	Center	.33	2.0	.34	.38	1.65	.41	.37
ABS-C	A	Edge	.27	2.0	.33	.52	1.66	.40	1.30
	B	Edge	.16	2.0	.33	JO	1.68	.40	1.25
	C	Edge	#	#	.33	#	#	.40	#

Solution did not converge at failure pressure

Table 5 Predicted failure data

Material	Geometry	PREDICTED FAILURE DATA		ACTUAL FAILURE DATA		RATIOS
		Burst Pressure	Location of Failure	Burst Pressure	Location of Failure	Actual Burst Pres. / Predicted Burst Pres.
304 S.S.	A	12,300 PSI	Edge	15,000 PSI	Edge	1.22
	B	4,800 PSI	Edge	6,800 PSI	Center	1.42
	C	7,400 PSI	Center	7,700 PSI	Center	1.04
A-533 B	A	9,800 PSI	Edge	11,000 PSI	Edge	1.12
	B	4,200 PSI	Edge	5,300 PSI	Edge	1.2
	C	6,800 PSI	Center	6,700 PSI	Center	.99
ABS-C	A	8,000 PSI	Edge	9,800 PSI	Edge	1.23
	B	3,000 PSI	Edge	3,750 PSI	Edge	1.25
	C	---	---	4,940 PSI	Edge	---

6 Langer, B. F., "Design-Stress Basis for Pressure Vessels, The William M. Murray Lecture," 1970; *Experimental Mechanics,* Jan. 1971.

7 Langer, B. F., "Fatigue Evaluation for Primary-Plus-Secondary Stresses Which Exceed $3S_m$," Westinghouse Nuclear Energy Systems, June 1969.

8 Davis, E. A., and Connelly, F. M., "Stress Distribution and Plastic Deformation in Rotating Cylinders of Strain-Hardening Material," *Journal of Applied Mechanics,* TRANS. ASME, Vol. 26, 1959, pp. 25–

9 Davis, E. A., "Yielding and Fracture of Medium Carbon Steel Under Combined Stress," *Journal of Applied Mechanics,* TRANS. ASME, Vol. 67, A-13, Mar. 1945.

10 Siebel, E., and Maier, A., "Der Einfluss Mehrachsiger Spannungszustande auf das Formanderungsvermogen Werkstaffe," *Zietschrift V.D.I.,* Vol. 77, Dec. 1933.

11 Marin, J., and Hu, L. W., "Plastic Stress Strain Relations for Biaxial Tension and Variable Stress Ratios," *Proceedings of A.S.T.M.,* Vol. 52, 1952.

12 Clausing, D. P., "Effect of Plastic Strain State on Ductility and Toughness," *International Journal of Fracture Mechanics,* Vol. 6, No. 1, Mar. 1970.

Printed in U. S. A.

Docket Number 50-346
License Number NPF-3
Serial Number 1-1280
Enclosure 2

COMMITMENT LIST

THE FOLLOWING LIST IDENTIFIES THOSE ACTIONS COMMITTED TO BY THE DAVIS-BESSE NUCLEAR POWER STATION (DBNPS) IN THIS DOCUMENT. ANY OTHER ACTIONS DISCUSSED IN THE SUBMITTAL REPRESENT INTENDED OR PLANNED ACTIONS BY THE DBNPS. THEY ARE DESCRIBED ONLY FOR INFORMATION AND ARE NOT REGULATORY COMMITMENTS. PLEASE NOTIFY THE MANAGER – REGULATORY AFFAIRS (419-321-8450) AT THE DBNPS OF ANY QUESTIONS REGARDING THIS DOCUMENT OR ANY ASSOCIATED REGULATORY COMMITMENTS.

COMMITMENTS	DUE DATE
None	N/A